NAVAL POSTGRADUATE SCHOOL

MONTEREY, CALIFORNIA

THESIS

A HYBRID ICEBREAKING RESISTANCE MODEL TO ACCOMMODATE DAMAGE TO THE ICE SHEET

by

David A. Bannish

June 2013

Thesis Advisor:	Young W. Kwon
Thesis Co-Advisor:	Jarema M. Didoszak

Approved for public release; distribution is unlimited

THIS PAGE INTENTIONALLY LEFT BLANK

REPORT DOCUMENTATION PAGE			Form Approved OMB No. 0704–0188
Public reporting burden for this collection of information is estimated to average 1 hour per response, including the time for reviewing instruction, searching existing data sources, gathering and maintaining the data needed, and completing and reviewing the collection of information. Send comments regarding this burden estimate or any other aspect of this collection of information, including suggestions for reducing this burden, to Washington headquarters Services, Directorate for Information Operations and Reports, 1215 Jefferson Davis Highway, Suite 1204, Arlington, VA 22202–4302, and to the Office of Management and Budget, Paperwork Reduction Project (0704–0188) Washington, DC 20503.			
1. AGENCY USE ONLY ***(Leave blank)***	**2. REPORT DATE** June 2013	**3. REPORT TYPE AND DATES COVERED** Master's Thesis	
4. TITLE AND SUBTITLE A HYBRID ICEBREAKING RESISTANCE MODEL TO ACCOMMODATE DAMAGE TO THE ICE SHEET		**5. FUNDING NUMBERS**	
6. AUTHOR(S) David A. Bannish			
7. PERFORMING ORGANIZATION NAME(S) AND ADDRESS(ES) Naval Postgraduate School Monterey, CA 93943–5000		**8. PERFORMING ORGANIZATION REPORT NUMBER**	
9. SPONSORING /MONITORING AGENCY NAME(S) AND ADDRESS(ES) N/A		**10. SPONSORING/MONITORING AGENCY REPORT NUMBER**	
11. SUPPLEMENTARY NOTES The views expressed in this thesis are those of the author and do not reflect the official policy or position of the Department of Defense or the U.S. Government. IRB Protocol number ____N/A____.			
12a. DISTRIBUTION / AVAILABILITY STATEMENT Approved for public release; distribution is unlimited		**12b. DISTRIBUTION CODE**	

13. ABSTRACT (maximum 200 words)

An analytical framework was constructed to interchange ice resistance components from existing ice resistance calculation methods. Within this framework, the Lindqvist analytical method bending ice resistance component was substituted with a value obtained from a finite element static model of the ice sheet. A parametric study of this substitution was performed with error correction to within 12% over the entire range of parameter variation. The finite element ice sheet model was then damaged; and then the average ice bending resistance was obtained, substituted into the Lindqvist analytical method, and quantified as a change in the total ice resistance. Therefore, a hybrid ice resistance model was developed that accounts for the effect of damage to the bending resistance component, and enables further study of unconventional icebreaking methods.

14. SUBJECT TERMS Ice Resistance, Icebreaker			**15. NUMBER OF PAGES** 97
			16. PRICE CODE
17. SECURITY CLASSIFICATION OF REPORT Unclassified	**18. SECURITY CLASSIFICATION OF THIS PAGE** Unclassified	**19. SECURITY CLASSIFICATION OF ABSTRACT** Unclassified	**20. LIMITATION OF ABSTRACT** UU

NSN 7540–01–280–5500 Standard Form 298 (Rev. 2–89)
Prescribed by ANSI Std. 239–18

THIS PAGE INTENTIONALLY LEFT BLANK

Approved for public release; distribution is unlimited

A HYBRID ICEBREAKING RESISTANCE MODEL TO ACCOMMODATE DAMAGE TO THE ICE SHEET

David A. Bannish
Lieutenant Junior Grade, United States Coast Guard
B.S., U.S. Coast Guard Academy, 2009

Submitted in partial fulfillment of the
requirements for the degree of

MASTER OF SCIENCE IN MECHANICAL ENGINEERING

from the

NAVAL POSTGRADUATE SCHOOL
June 2013

Author: David A. Bannish

Approved by: Young W. Kwon
Thesis Advisor

Jarema M. Didoszak
Thesis Co-Advisor

Knox T. Millsaps
Chair, Department of Mechanical and Aerospace Engineering

THIS PAGE INTENTIONALLY LEFT BLANK

ABSTRACT

An analytical framework was constructed to interchange ice resistance components from existing ice resistance calculation methods. Within this framework, the Lindqvist analytical method bending ice resistance component was substituted with a value obtained from a finite element static model of the ice sheet. A parametric study of this substitution was performed with error correction to within 12% over the entire range of parameter variation. The finite element ice sheet model was then damaged; and then the average ice bending resistance was obtained, substituted into the Lindqvist analytical method, and quantified as a change in the total ice resistance. Therefore, a hybrid ice resistance model was developed that accounts for the effect of damage to the bending resistance component, and enables further study of unconventional icebreaking methods.

THIS PAGE INTENTIONALLY LEFT BLANK

TABLE OF CONTENTS

THIS PAGE INTENTIONALLY LEFT BLANK

LIST OF FIGURES

LIST OF TABLES

THIS PAGE INTENTIONALLY LEFT BLANK

ACKNOWLEDGMENTS

I wish to thank Prof. Kwon, Prof. Didoszak, and LT Gary Kim for their knowledge and enjoyable academic discussion.

I also thank the faculty and staff of the Naval Postgraduate School for their outstanding support contributing to the completion of this study.

THIS PAGE INTENTIONALLY LEFT BLANK

I. INTRODUCTION

A. ICEBREAKING HISTORY

Prior to the 20th century, the first true icebreaker, Yermak, was commissioned and tasked with exploring the polar regions of the globe. The vessel had a displacement of 10,000 tons, a 10,000 hp propulsion system consisting of three screws aft with one screw forward, thickened hull plating, double hull construction, a ballast system to quickly affect roll/trim, and a rounded hull form [1]. The summation of these design characteristics ensured this to be the first vessel to reliably transit multi-year sea ice, which it did from 1899 to 1963. The success of this ship ultimately defined the specifications for the IACS Polar Class of vessels, from which all modern icebreakers are derived [2]. As a result of this tried and true formula for immensely powerful and specialized ice navigation platforms, the overall ship design and mechanical process to break ice is essentially the same today as it was back then. Despite this similitude, the icebreaker underwent several design iterations, and efficiency is considerably improved over 1899 as the concept was refined and matured.

Substantial research was also conducted to develop systems to damage ice ahead of the icebreaker such that the ice failed with less effort from the ship. This concept was successfully used to aid early expeditions to the Antarctic, by fracturing the ice with explosives. Less violent means of damaging ice, such as water jet cutting mechanisms, were conceived to provide the benefit of the explosives with the practicality of a shipboard system. The Yermak served as the test bed for the first water jet cutters aboard icebreakers sometime after the idea was introduced in 1935 [3]. The water jets at that time lacked the power density and peak pressures to provide any benefit to the icebreaker. At the time the Yermak was retired in 1963, follow on research attempted to physically model the effectiveness of an icebreaker with ice cutting systems [3]. The significant disparity between the failure characteristics of model and full scale ice resulted in criticism that the claims of this report were too optimistic in favor of ice cutting systems, and more specifically, water jet cutters [4]. Nonetheless, the greatest

contribution of this work was the desire to use modeling methods to craft new strategies to damage the ice and allow the passage of a ship.

From literature review, two themes following the 1963 study became apparent. First, the efficiency of the ice cutting systems received detailed study [4]-[8].Second, much research was done to adequately define the material properties of ice [9], [10], and apply this to reasonably model the icebreaking process [11], [12]. With minor exception [3], the research tended to ignore the application of these icebreaking systems in terms of a grander icebreaking strategy. In other words, the specific damage pattern that causes ice to most readily fail in the presence of the icebreaker received little attention. Just as the summation of its parts cemented the Yermak's title as the first true icebreaker, the effectiveness of the ice breaking / ice cutting system relies on the synergy between the available tools and their artful manipulation.

B. STUDY OBJECTIVE

This study combines the advantages of existing ice resistance calculation methods into a single hybrid method, such that the steady state velocity of an icebreaker is correlated to the available thrust; and include cases in which the ice sheet possesses some artificial damage. In addition, this study intends to demonstrate the utility of this hybrid model by rationalizing ice resistance estimates against other modeling techniques, full power test results, and realistic performance of modern ice cutters.

II. BACKGROUND

A. DEFINITIONS

To more appropriately convey the subject material, all pertinent variables are hereby defined in Tables 1–5. All equations obtained from literature or developed are based on these definitions to aid consistency in presentation. Table 1 provides the unit vectors for two body-fixed coordinate frames. The icebreaker reference frame is given in Cartesian coordinates. The icebreaking surface frame is defined in two dimensions and is coupled to the icebreaker reference frame. The parameters and dynamics for the icebreaker are provided in Table 2. All parameters are typically known after the initial design stage. The icebreaker body has six degrees of freedom; three translational motions, and three rotational motions. This study emphasizes forward translation of the icebreaker only within this context, although follow on study should include additional motions. The parameters of sea ice including dimensional, material property, and material failure considerations are provided in Table 3. All physical parameters and variables for existing analytical ice resistance methods are included in Table 4. All parameters affecting the development and error of the hybrid method for average ice bending resistance are included in Table 5. An illustration of the reference frames, hull parameters, and motions are provided in Figure 1.

Table 1. Body-fixed coordinate system conventions.

Reference Frame		
Coordinate System	**Unit Vector**	**Definition**
Icebreaker Body-Fixed	X	longitudinal
	Y	transverse
	Z	vertical
Hull-Ice Contact Surface	n	normal
	t	tangential

Table 2. Icebreaker parameters and motions variable definitions.

Icebreaker		
Parameters	**Variable**	**Name**
	Δ	displacement
	M	mass
	Ps	shaft power
Dimensions	L	length at waterline
	B	breadth
	T	draft
Bow Angles	α	waterline entrance
	β	flare
	γ	stem
	ζ	effective ice contact
Dynamics	**Variable**	**Motion Affected**
Translation	x	surge
	y	sway
	z	heave
Rotation	θ	roll
	ϕ	pitch
	ψ	yaw

Table 3. Sea ice parameters.

Sea Ice		
Parameters	**Variable**	**Name**
Dimensions	d	grain diameter
	H	thickness
	lc	characteristic length
	l	cusp length
	w	cusp width
	R	cusp radius
	Ro	cusp radius reference
	η	cusp radius angular position
Properties	E	Young's modulus
	ρice	density
	ν	Poisson's coefficient
	μ	friction coefficient
	νa	air concentration
	νb	brine concentration
	Ω	temperature
Material Failure	σb	bending stress
	σb,o	uncorrected bending stress
	σc	crushing stress
	τs	shear stress
	σ1	principle stress
	σ2	principle stress
	dσ/dt	stress rate
	δσ1/δx2	stress gradient
	C	stress rate constant
	D	stress gradient constant
	K	stress gradient limit

Table 4. Physical parameters and resistance component variable definitions.

Resistance Calculation		
Parameters	**Variable**	**Name**
	ρw	sea water density
	Fp	propulsion force
	Fv	vertical ice loading force
	g	gravitational acceleration
	n	number of cusps
	V	velocity
	Vi	initial velocity iterate
	Vi+1	product velocity iterate
Resistance	Rb	bending resistance
	Rc	stem crushing resistance
	Rice	ice resistance
	Row	open water resistance
	Rr	rotation resistance
	Rs	submergence resistance
	Rsf	skin friction resistance
	Rw	wavemaking resistance

Table 5. Hybrid method parameters for average ice bending resistance.

Finite Element Bending Resistance		
Parameters	Variable	Name
	A	FEM proportionality constant
	b	error slope-intercept
	F	distributed ice loading force
	m	error slope
	N	parameter power constant
	p	substitute parameter

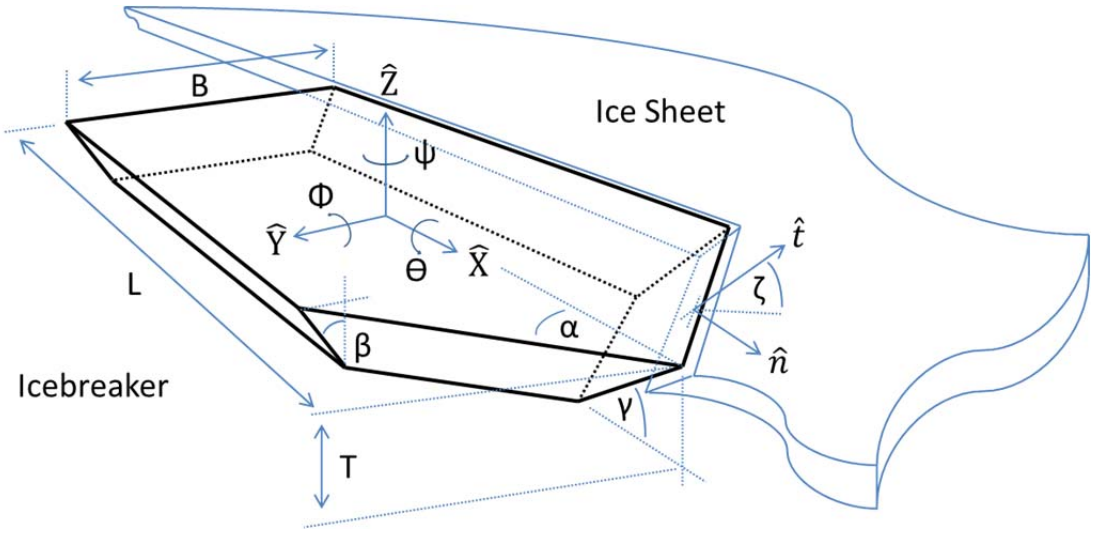

Figure 1. Illustration of Icebreaker Conventions

B. LITERATURE REVIEW

1. Sea Ice Properties

Accurate ice resistance models require knowledge of sea ice material properties and failure mechanisms in the presence of an icebreaking ship. However, the material properties of sea ice are difficult to assign because many studies identify variations in ice samples based on age, chemical composition, temperature, scale, and testing method [9]. For example, in the Lindqvist 1989 study [13], nearly one order of magnitude variation in the flexural failure stress of ice was observed during in-situ testing. Therefore, the material properties obtained from literature are approximate quantities, and likely require refinement based on further specification of these variables.

Sea ice is formed from accumulated snow at the surface of seawater, and has a microstructure that differs considerably from freshwater ice. Sea ice typically assumes a hexagonal column structure with anisotropic material properties. Unlike freshwater ice, which forms a uniform crystalline structure, the grains in sea ice orient in several directions, lending to the formation of an ice sheet with varying thickness. Additionally, brine channels form between the grains, forming a heterogeneous solid solution within the ice sheet, and giving the ice viscoelastic properties. Repeated tests indicate either ductile or brittle material failure depending on the ice temperature, composition, and stress rate [9].

a. Density

The density of sea ice is roughly approximated as 910 kg/m^3 [9].

b. Young's Modulus

Given the viscoelastic behavior of sea ice, Young's Modulus varies from 0.3 GPa-10 GPa for static loads, to 6 GPa-10 GPa for dynamic loads [9].

c. Poisson's Ratio

The Poisson's ratio is approximately 0.295 [9], although it is also presented as 0.3 [9].

d. Flexural Strength

(1) Temperature

The flexural strength is related to the temperature of the ice for temperatures -0.4 C > Ω > -18.5 C [9].

$$\sigma_b = 4.7 - 0.96\Omega - 0.31\Omega^2 \tag{2.1}$$

(2) Composition

The expression for flexural strength as a function of composition is shown below, where ν_a is the concentration of air, and ν_b is the brine concentration [9].

$$\sigma_b = \sigma_{b,o}\left(\nu_a, \nu_b\right) \tag{2.2}$$

(3) Stress Rate

The flexural strength of the ice has no dependence on stress rate in the range 49.0 kPa/s < < 981 kPa/s. For flexural stress rates above 981 kPa/s, the flexural strength is obtained as a function of the stress rate [9].

$$\sigma_b = \sigma_{b,o} + C \ln \frac{d\sigma}{dt} \tag{2.3}$$

(4) Testing Method

Depending on either a small beam or ring tensile test for ice, the tensile stress of ice was measured at 0.785 MPa and 1.77 MPa, respectively [9].

(5) Grain Diameter

The flexural stress of ice is approximated as a function of the grain diameter, typically between 1 cm and 2 cm [9].

$$\sigma_b = \frac{1.11}{d} \tag{2.4}$$

Where the grain diameter, d is given in centimeters, and the flexural stress, σ_b is in MPa.

e. Shear Strength

The shear test estimates the shear failure stress at 2.06 MPa [9].

f. Compressive Strength

Compressive failure of the ice varies by orientation of the ice crystal, having a maximum of 8.34 MPa for cores loaded on the principle axis, and a minimum of 3.43 MPa for cores loaded perpendicular to this principle axis [9].

g. Stress Gradient

In addition to these three failure mechanisms, sea ice fails at a stress gradient threshold [10].

$$K^2 = \left(\sigma_1 - \sigma_2\right)^2 + \sigma_1^{\,2} + \sigma_2^{\,2} - D\left(\frac{\partial \sigma_1}{\partial x_2}\right)^2 \tag{2.5}$$

This equation modifies the von-Mises plane stress failure criterion to include the stress gradient term, the partial derivative of the principle stress with respect to the perpendicular axis.

2. Icebreaking Process

Icebreakers induce failure of the ice by three observed mechanisms; crushing, shearing, and flexure. In most icebreaking operations, all three of these mechanisms are

present to some degree. Crushing and shear failure are localized at the hull-ice contact area, whereas flexural failure occurs at some distance from the icebreaker. The general pattern of damage generated by an icebreaker is a crushing zone at the stem of the icebreaker, with the formation of characteristic semi-elliptical cracks, known as cusps, from the centerline to the extreme breadth, caused by flexural failure. The cusps may also exhibit secondary crack formation from the contact surface radially along the length of the cusp [13]-[16].

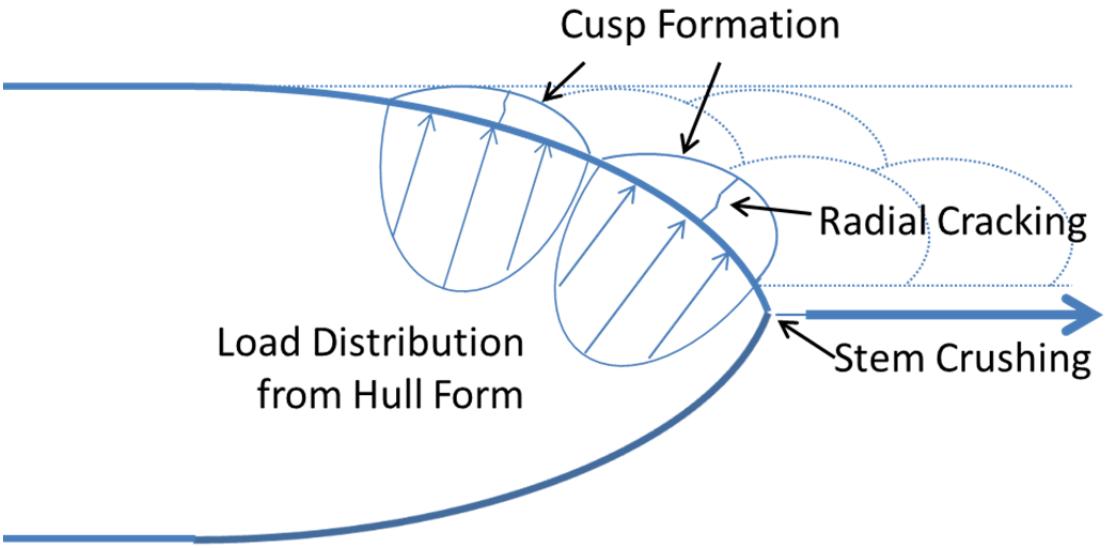

Figure 2. Illustration of icebreaking process.

As a result of the material properties of sea ice, this pattern of cusp formation is dependent on icebreaker dynamics, as observed in laboratory and scale-model testing [15]. In certain conditions, the ice cusps occur predictably at specific locations along the bow. However, past research cannot conclude whether icebreaker dynamics are beneficial or detrimental to the overall ice resistance [15]. In addition, the interplay of failure mechanisms is dependent on the dimensions of the ice due to stress gradient limitations [10]. Upon failure of the ice, the icebreaker clears the ice underneath and to either side. In this stage, the icebreaker both rotates and submerges the broken pieces, providing some resistance to the ship. However, as the broken pieces are no longer providing structural resistance from the ice sheet, the thrust exceeds the resistance forces, and the icebreaker

regains momentum. To maintain transit speed through the ice, all momentum lost by the loading of the ice must be restored within a distance equal to the length of the broken pieces in the direction of motion, before the icebreaker once again encounters the ice sheet [16].

3. Model Techniques

Since icebreaking ships traditionally represent significant capital investment, modeling is conducted to allow iterative performance improvements to the intended design. Three types of modeling were developed, each with inherent advantages and disadvantages depending on the application. The three types of models are; scale models, analytical models, and numerical models.

a. Scale Models

Similar to tow tank testing, this modeling technique incorporates a layer of model ice floating on top of the water. The desired hull form is constructed, instrumented, and physically tested while breaking model ice. This technique is advantageous because resistance data is obtained directly, according to scale, and involves physical failure of the sea ice. The major caveat to this advantage is that the stress gradient, stress rate, and complex composition of sea ice disrupt the accuracy of the scale results. To more accurately simulate the full scale icebreaking process, the model ice is either "doped" by adding chemicals to affect the material properties, or is manufactured similarly to natural sea ice by allowing artificial snow to freeze on the tow tank surface [15]. Despite realistic interpretation of full scale icebreaking operations, the disadvantage to this method is that it is not practical at the initial design stages because of cost, time, and facilities availability.

b. Analytical Models

In contrast to scale modeling, analytical models [13], [14] are useful to calculate ice resistance at the initial design stages because of their simplicity. For ships following the general specifications of a modern icebreaker, existing analytical models

are the most practical means to determine ice resistance. Since analytical models are constrained by a certain set of assumptions for a particular method, a major disadvantage of a semi-empirical analytical model is that results are scaled with respect to existing similar ships analysis, and may not provide reasonable performance estimation for more radical ship designs. Even with a standard hull form, in the case of the ice cutting ship, current analytical methods are constrained to local ice failure, and cannot account for the effect of damage to the ice sheet at some distance from the icebreaker. However, one trait of analytical methodology is the decoupling ice resistance into various constituents. For example; open water resistance, bending resistance, crushing resistance, rotational inertia resistance, and submergence resistance may be solved for separately, according to approximate system parameters, and scaled to match empirical data. Therefore, it is feasible that some modification of particular resistance constituents within the analytical method may allow inclusion of ice sheet damage to the overall ice resistance calculation.

c. Numerical Models

While finite element models have the potential to replicate the physical phenomena of breaking ice, these models encompass a wide range of programs with varying complexity and accuracy. Numerical methods have already implemented variable parameters and dynamics affecting icebreaking processes [17]-[19]. However, the inherent imperfections and nonlinearity of the solution of the numerical model requires validation with empirical data across the entire range of expected operations, adding to the cost of the technique. Although numerical models may provide insight into new radical icebreaker designs at marginal expense, they may also contain significant unforeseen errors that must be accounted for by other means.

4. Cusp Geometry

Several research efforts attempt to relate ice cusp dimensions to the ice loading because of its significant influence on ice resistance predictions. As a result, three types of ice cusp approximations were obtained from literature, with varying application and accuracy describing this form of damage realistically. In order of complexity, ice

cusps were analyzed according to one-dimensional, two-dimensional orthogonal, and two-dimension radial coordinate systems as shown in Figure 3. Within this spectrum of analysis, the ice is either uniformly loaded along the edge, or experiences point loading. The relative accuracy of each depends on the geometry of the hull. Since uniform loading is expected of bows with flat contact surfaces, such as the Thyssen-Waas bow, the uniform loading analysis can reasonably describe the icebreaking pattern. For other bow forms with some curvature, however, point loads are a more realistic assumption. In all of these cases, the ice is assumed as a homogeneous and isotropic sheet of uniform thickness with perfectly vertical edges on a uniform elastic foundation.

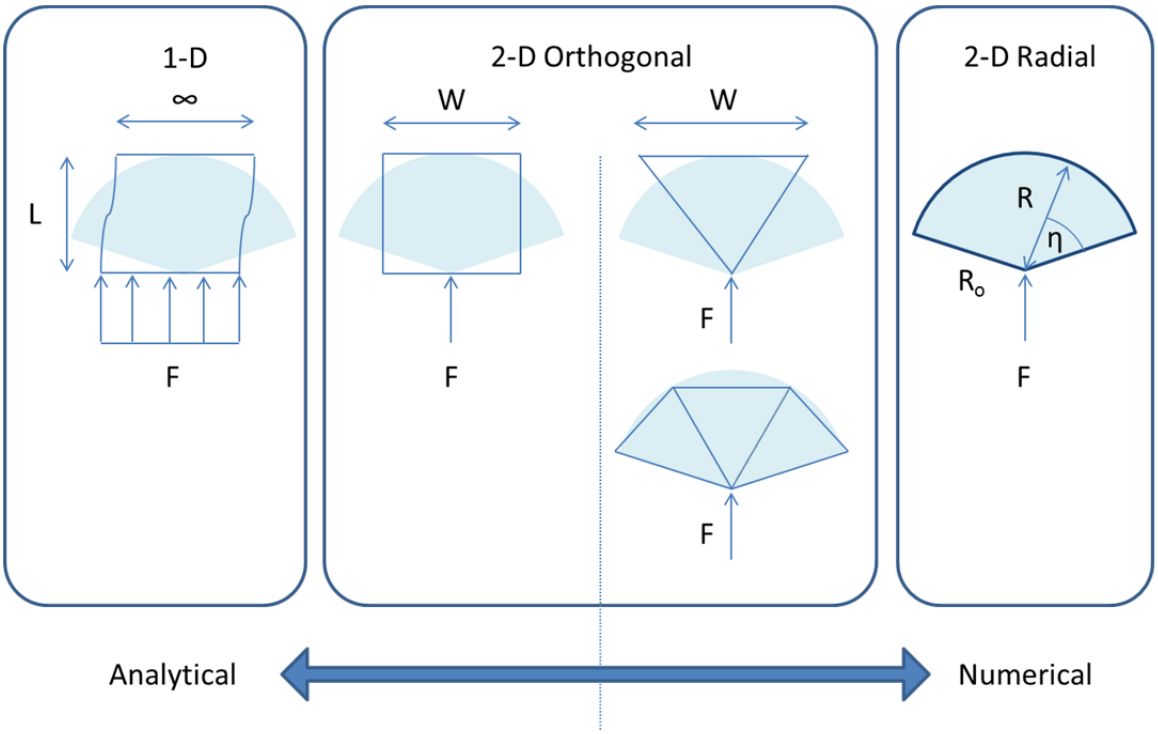

Figure 3. Illustration of cusp approximation methods.

a. One Dimensional

The least complex form of ice cusp analysis assumes the ice sheet as a semi-infinite plate loaded along a single free edge. In this form, the ice is assumed to fail at a set distance from the free edge of the plate, proportional to the characteristic length of the plate, *lc* [13].

$$l_c = \left[\frac{E H_{ice}{}^3}{12\left(1-\nu^2\right)\rho_w g} \right]^{\frac{1}{4}} \tag{2.6}$$

This distance from the edge to the location of failure is referred to as the cusp length. Since this method fails to account for the cusp width, two issues arise that affect its application. First, it is difficult to derive a realistic physical association between the assumed distributed load required for cusp failure and the point load it represents. Second, the cusp length determined by this method is likewise restricted to one-dimensional applications. Therefore, such analysis is best suited to cases exhibiting: 1) distributed loading of the ice sheet, and 2) the width of the distributed loading is much greater than the cusp length. For the majority of icebreakers, however, this method is not reliable.

b. Two Dimensional Orthogonal

There are two variations of this method, constituting the progression from a distributed load to a point load assumption. This is accomplished by assuming specific failure shapes according to prescribed geometries, in which the orthogonal cusp width is related to the cusp length. The cusp shapes are defined by either rectangular or triangular elements, as shown in the figure. In all cases, the cusp length is determined by the same method as the one-dimensional analysis. It is important to note that several analytical icebreaking resistance methods combine the rectangular and triangular elements, therefore, accepting a significant departure from both the natural icebreaking process and analytical description.

(1) Rectangular Element

This variation is similar to the one-dimensional method, except that the cusp width is related to the cusp length. This allows the frequency of ice cusp formation to be determined, thus improving the accuracy of the total ice load approximation, with marginal increase in calculation. However, as in the one-dimensional case, it is difficult to assign an appropriate loading force that bears physical compatibility.

(2) Triangular Element

This variation relates the length of the cusp as sides of an isosceles triangle to an arbitrarily determined base, the cusp width. This allows the cusp to be solved in the same

manner as the rectangular cusp, with exception of variable cross-section along the cusp length. However, since the free edge is infinitely small, the distributed force acting on this representative cusp may be approximated as a point load. In addition, these triangular cusps may be joined side by side to form a cusp resembling a semi-circle experiencing a point load at the center. If an infinite number of triangular elements are used, the error between the cusp shape and triangular representation can be effectively eliminated. Therefore, this variation allows both versatile and somewhat realistic description of the cusp. However, the solution complexity limits it to numerical solvers [20].

c. Two Dimensional Radial

The most complex, and likewise, accurate methods for determining the relationship between the ice loading force and semi-elliptical cusp dimensions appropriately analyze the system in a two-dimensional radial system. Similarly to the triangular cusps, the ice is loaded at a single point. Since the relationship obtained from literature has empirical basis, it is much more easily calculated upon determining the cusp variables. The caveat to this, however, is that a numerical solver is required to determine all variables [18].

THIS PAGE INTENTIONALLY LEFT BLANK

III. LINDQVIST METHOD

A. REASON FOR COMPARISON

The Lindqvist method for calculation of ice resistance is a semi-empirical analytical model that is referenced by several modern ice resistance methods as a standard for comparison [16], [21], [22]. The Lindqvist method likewise serves as a benchmark for this particular study, although follow on research indicates that the method likely has some conservative error. Therefore, the hybrid ice resistance method is developed out of respect to the Lindqvist method, adopts components of this method to reduce error in comparison, and attempts to make improvements to experimental error.

B. ASSUMPTIONS

Several assumptions were made in the development of the Lindqvist method that affects the accuracy of the solution. These assumptions fall into two general categories, those that are in place to eliminate nonlinearity from the method, and those that provide rough approximation for poorly understood quantities. The empirical basis and linearity of the method allow it to be reasonably accurate, despite room for improvement within the individual assumptions. The assumptions of the Lindqvist Method are as follows:

1. Linear Assumptions

- Ice resistance increases linearly with velocity.
- The vessel is motionless with exception of constant forward translational velocity.
- The hull is approximated as a plane, developed from average hull angles, exerting normal and tangential force components on the ice at the waterline.
- Upon contact, the ice fails instantaneously.
- The failed ice pieces do not provide rotational inertia resistance back to the hull, nor are they affected by the viscosity of the water.
- The ice does not exhibit viscoelastic, stress rate, or stress gradient properties.

2. Quantity Assumptions

- Broken ice provides frictional resistance evenly distributed along 70% of the underside of the hull once submerged.
- The resistance force is independent of the crushing failure stress.
- The shear failure stress equals the bending failure stress.
- Young's modulus for ice is 2 GPa.
- Poisson's ratio for ice is 0.3.
- Friction coefficient during hull-ice interaction is 0.1 for hulls with low-friction coatings and 0.16 otherwise.
- Both the length and width of a failed ice cusp are equal to one third of the characteristic length of an edge-loaded semi-infinite plate with uniform elastic support.

C. RESISTANCE COMPONENTS

1. Stem Crushing

The equation derived to approximate the stem crushing resistance is provided below. The equation is multiplied by an approximate proportional constant obtained by instrumenting the bow of the icebreaker with strain gauges, and taking transient measurements with reference to the ice bending failure stress and thickness. It is important to note that this resistance is not influenced by the dimensions of the icebreaker.

$$R_c = 0.5\ \sigma_b\ H_{ice}{}^2 \frac{\left[\tan\gamma + \mu\frac{\cos\gamma}{\cos\zeta}\right]}{\left[1 - \mu\frac{\sin\gamma}{\cos\zeta}\right]} \tag{3.1}$$

where the effective ice contact angle ζ, between the hull and the ice, is defined as a function of the waterline entrance and stem angles.

$$\zeta = \tan^{-1}\left[\frac{\tan\gamma}{\sin\alpha}\right] \tag{3.2}$$

2. Bending

The bending resistance equation assumes the failure of a non-integer number of ice cusps with dimensions proportional to the characteristic length of the ice sheet, modeled as a semi-infinite plate supported on an elastic foundation.

$$R_b = 0.003\ \sigma_b B\left(\frac{H_{ice}^{1.5}}{\sqrt{\rho_w g}}\right)\left[\tan\zeta\left(\frac{\mu\cos\gamma}{\sin\alpha\cos\zeta}\right)\right]\left(1+\frac{1}{\cos\zeta}\right) \tag{3.3}$$

3. Submergence

The submergence resistance component provides the frictional contribution of the broken ice flows as a function of the approximated underwater surface area of the hull and submerged depth. This formulation incorporates the snow thickness resting on top of the ice because this is also submerged. This equation does not explicitly consider the influence of the added mass of water surrounding the ice chunks as they are submerged.

$$R_s = \left(\rho_w - \rho_{ice}\right) g\left(H_{ice} + H_{snow}\right) B\left[T\left(\frac{B+T}{B+2T}\right) + \mu k\right] \tag{3.4}$$

where

$$k = \left(0.7L - \frac{T}{\tan\gamma} - \frac{B}{4\tan\alpha} + T\cos\gamma\cos\zeta\sqrt{\frac{1}{\sin\gamma^2} + \frac{1}{\tan\alpha^2}}\right) \tag{3.5}$$

D. EMPIRICAL VELOCITY RELATION

As Lindqvist observed, measured ice resistance appears to increase linearly with velocity from some nonzero resistance value as expressed below.

$$R_{ice} = \left(R_c + R_b\right)\left(1 + 1.4\frac{V}{\sqrt{gH_{ice}}}\right) + R_s\left(1 + 9.4\frac{V}{\sqrt{gL}}\right) \tag{3.6}$$

The Lindqvist empirical velocity relation accounts for this observation by setting the zero-velocity resistance as the sum of the three resistance components, and increasing the value of each component linearly according to velocity, and scaling these values according to non-dimensional constant values. Thus, this velocity relation implies that two criteria must be met. First, assuming a linear relation between ice resistance and

velocity as observed, the three resistance components must equal the predicted zero-velocity slope-intercept of the empirical resistance data. Second, the contribution of each resistance component must be scaled appropriately with velocity, such that the sum of three resistance components equals the total resistance for a range of vessels.

E. INTRINSIC VALIDATION

The Lindqvist method was validated against both the calculated and empirical resistance data extrapolated from the original study. This comparison was necessary to ensure that the method was implemented properly into this study, since the Lindqvist resistance is typically presented as the total resistance, without specifying the contributions of the underlying resistance components. As desired, the resistance values calculated by Lindqvist were successfully reproduced for each vessel in the original study. Therefore, the individual resistance components analyzed by Lindqvist during the formation of his method were likewise reproduced, as shown in Figure 4.

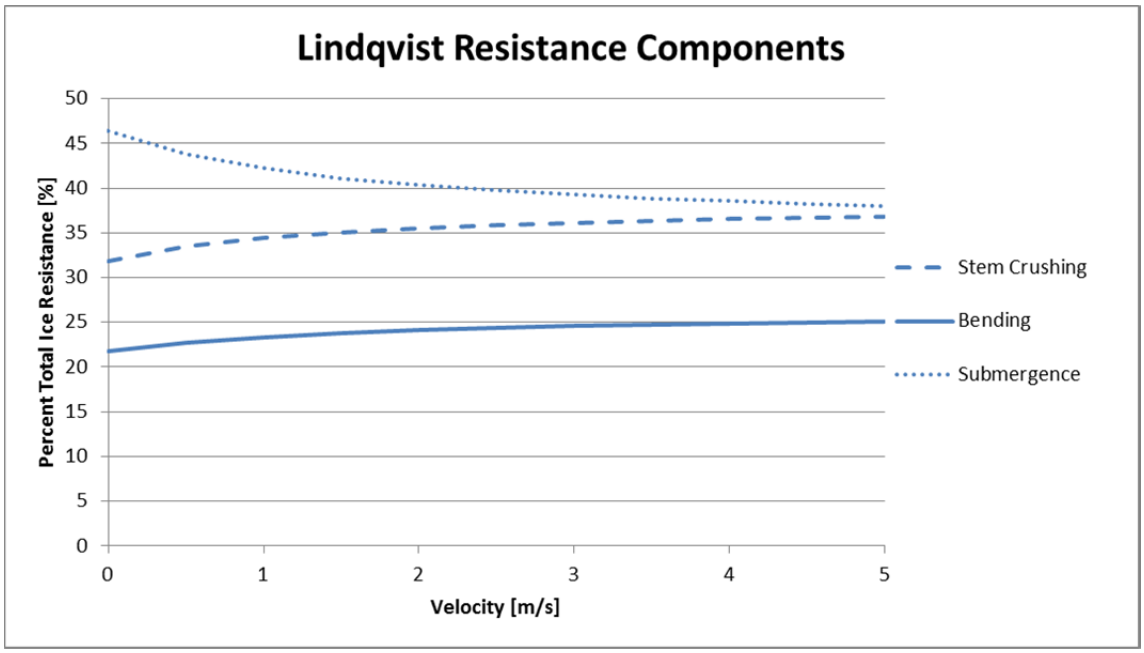

Figure 4. Relative influence of Lindqvist resistance components on the icebreaker Vladivostok with respect to velocity.

This analysis provided several insights into limitations of the method. Although the final empirical velocity relation achieves reasonably accurate calculation of the total ice resistance, there may be substantial errors in the individual resistance components. For example, the average resistance component values were obtained and compared with the total resistance versus vessel velocity. This indicated that although ice resistance appears to increase linearly with velocity, the contributions of the stem crushing and bending resistance components increase, while the submergence resistance component decreases. In addition, the relative contributions of each of these three resistance components were compared. Averaging from 0 m/s to 5 m/s, ice submergence provides approximately 40% to the total resistance, stem crushing provides 35%, and bending contributes 25%. Therefore, these percentages allow initial approximations of the ice resistance for icebreakers designed to eliminate any one component.

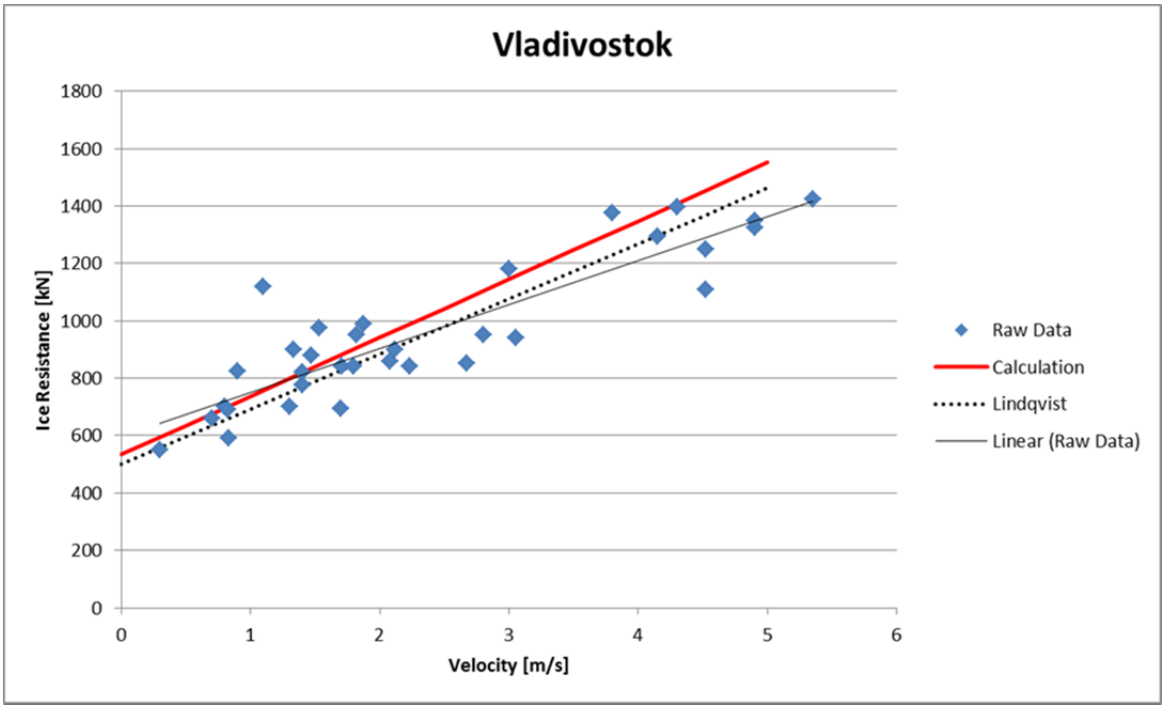

Figure 5. Extrapolated raw data for the icebreaker Vladivostok comparing the original Lindqvist ice resistance calculation with a calculation using the method and the best fit line of the data.

Using the extrapolated data, and assuming a linear resistance velocity relationship, a best fit line was drawn from the raw data, as shown in Figure 5, since this was not provided in the original study. Overlaying the Lindqvist calculation over the raw data and best fit line revealed that although the Lindqvist data reasonably approximates the resistance, the zero-velocity resistance, nor the slope of the resistance line are properly matched by the method. This was expected from the assumptions of the method and analysis over a range of vessels, however, these errors may also stem from the absence of a pertinent resistance component, such as rotation of the ice.

F. SENSITIVITY ANALYSIS

Successful implementation of the Lindqvist method enabled sensitivity analysis to determine the most influential variables on total ice resistance with regard to the individual resistance components, located in Appendix A. Table 5 lists the parameters used for the sensitivity study of each ice resistance component.

Table 6. Resistance component influential parameters

	Rc	Rb	Rs
L			x
B		x	x
T			x
α	x	x	x
γ	x	x	x
H	x	x	x
σ_b	x	x	
μ	x	x	x
E		x	
υ		x	
Δρ			x

Lindqvist acknowledges that some portions of the method require improvement, therefore this analysis contains errors. Since Lindqvist also indicates that his method is more accurate for larger vessels, the largest vessel of the original study, Vladivostok, was selected to mitigate these errors. As expected, the sensitivity analysis determined that the ice resistance is highly dependent on the vessel gross dimensions. bow angles, and the ice

dimensions. However, the Lindqvist method proved highly sensitive to the bending stress of the ice and the density differential between sea water and sea ice. This dependence on environmental variables requires that ice resistance calculations adequately describe the intended operating environment. Although the Lindqvist study described the bending stress for all cases, it did not describe the density differential. After several iterations, the best error obtained from adjusting the density differential was to within 10% of the original study. Therefore, the exact value of the density differential was not reproduced, but was close enough to proceed with analysis.

THIS PAGE INTENTIONALLY LEFT BLANK

IV. HYBRID METHOD DEVELOPMENT

The proposed hybrid method attempts to evaluate both conventional and other icebreaking strategies by achieving synergy among all modeling methods. The creation of this tool is motivated by the desire to perform objective icebreaking resistance analysis under a common framework, as shown in Figure 6. This framework is intended to provide the context to combine resistance components from multiple sources to determine the overall resistance. Comprehensive analysis of this method is not possible within the scope of this thesis because of its many variations across the range of all resistance approximation methods. Therefore, the proposed system requires further analysis, refinement of individual resistance components, and their relations.

A. PROPOSED FRAMEWORK

1. Resistance Components

Research was conducted to determine all analytical resistance components from literature, listed below.

- Bending
- Rotation
- Skin Friction
- Stem Crushing
- Submergence
- Wave Making

2. Icebreaking Functions

Separation of resistance components was accomplished by first subdividing the icebreaking process into three necessary functions; breaking the ice, clearing the ice, and making headway.

a. Icebreaking

The stem crushing and bending resistance components are included within the icebreaking function because these resistance components are only applied as the

icebreaker comes into contact with the ice sheet although these resistance components are often summed as steady values, they are actually cyclical depending on the failure of the ice due to the failure of the ice extending some distance ahead of the icebreaker. The stem crushing component provides more steady resistance to the icebreaker since the stem is the first part of the icebreaker to contact the ice, and is relatively unaffected by cusp failure. The bending component cyclical frequency, on the other hand, is highly dependent on the dimensions of the ice cusps.

b. Ice Clearing

The clearing of broken ice involves rotation and translation of the broken chunks. This function is accomplished by the rotation and submergence resistance components existing in literature. The rotation ice resistance component is a function of both the rotational moment of inertia of the failed ice cusp and the icebreaker velocity. The submergence resistance component incorporates both the translation of the broken ice under the water and the hull-ice contact friction, however, these may also be separated.

c. Hydrodynamic Resistance

Progressing relative to the ice sheet also involves making headway relative to the water beneath the ice. This relative motion creates drag on the icebreaker body in the form of frictional and pressure drag. The skin friction resistance component is directly proportional to the surface area of the hull in contact with the water. The pressure differential generates waves through this medium at the water-air interface. This drag component is defined in literature as the wave making resistance. Since the skin friction and wave making resistance components are traditionally of great importance ship design, they are typically obtained as a coupled resistance from scale model tow tank testing, but may be accounted for separately by a wide range of other methods.

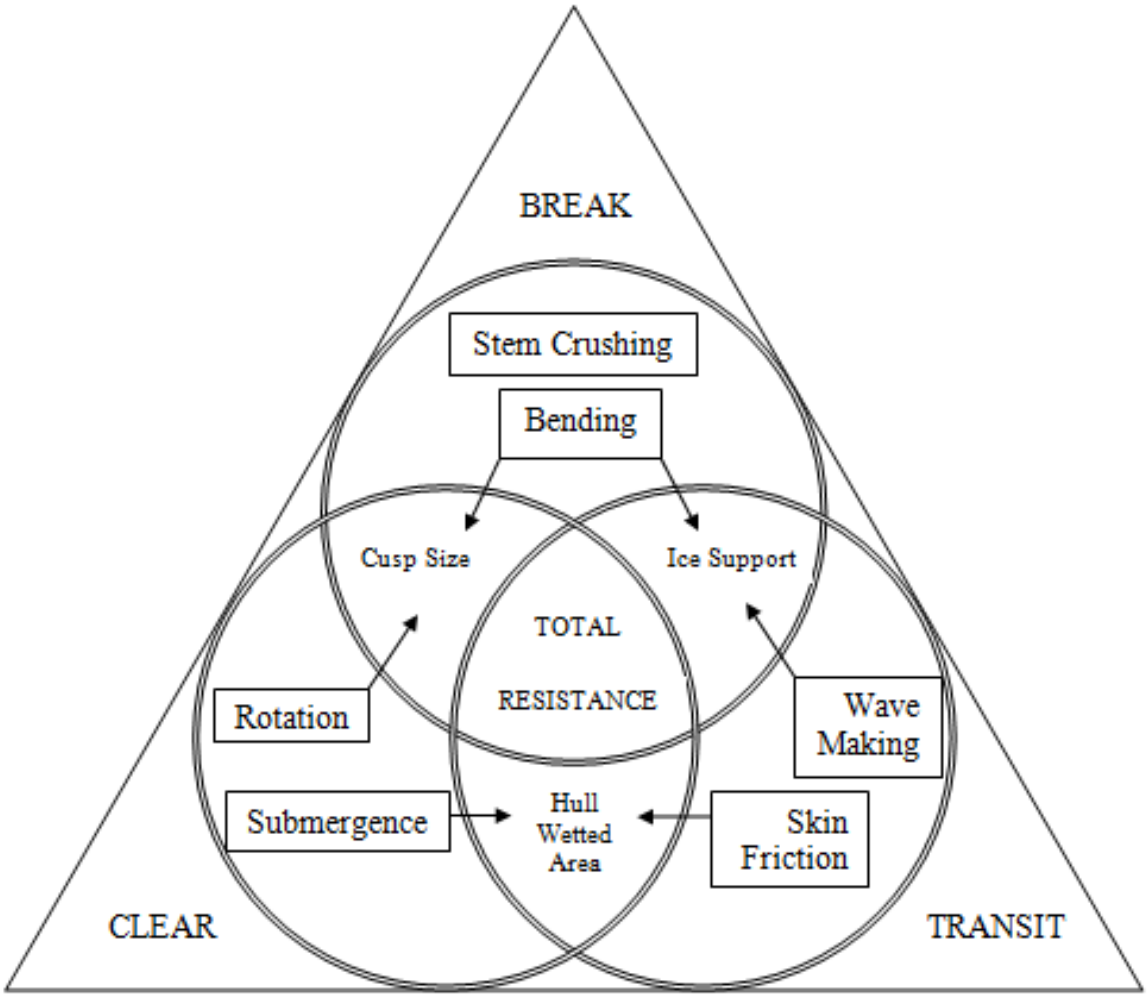

Figure 6. Proposed icebreaker resistance framework. The corners of the triangle represent the three icebreaking functions. The Venn-diagram illustrates the icebreaking resistance components obtained from literature. The arrows indicate potential relationships between resistance components.

B. ANALYTICAL VALIDITY

1. Resistance Coupling

The success of this method is governed by the validity of the assumption that the icebreaking process is comprised of discrete resistance components. This assumption is not particularly radical since the resistance components within the framework were all obtained from literature, and have been implanted into existing resistance models successfully [13], [16], [18]. However, Figure 6 also identifies cases, both described in

literature and newly added, in which some resistance elements are coupled. In the broader sense, this illustrates the interdependence of the three icebreaking functions. The first such coupling was observed in previous research, that hydrodynamic forces resulting from the motion of the icebreaker contributed to failure of the ice by affecting the buoyant force supporting the ice sheet [16]. This has also been observed during high speed icebreaking by hovercraft [6]. The remaining three instances of coupling are speculated in this study. The first speculates that the bending and rotation resistances are linked by the geometry of the failed cusp. The second potential relationship links the submergence and hydrodynamic skin friction components by the finite wetted hull area. The third assumes that there is some connection between stem crushing and bending components based on the dimensions and form of the bow.

2. Coupling Mitigation

This lack of information provided the motivation to speculate which parameters influence this coupling such that analytical errors are reduced or expected.

a. Velocity

The wave making and skin friction resistance values become trivial as velocity approaches zero. Since these values also contribute to coupling of the bending and submergence components, respectively, it is reasonably assumed that analytical error is reduced as velocity approaches zero. The zero-velocity assumption does not have serious implications on icebreaker operations since it produces the operating limits.

b. Hull Geometry

The stem crushing, bending, and rotation resistance components are effectively negated as the hull-ice contact angle approaches zero. However, these values remain coupled. Since the only design parameter not shared by all three of these components is the vessel breadth, this value may be adjusted to reduce expected analytical error. The stem crushing resistance component is independent of vessel breadth. Therefore, the stem crushing is effectively de-coupled from the bending resistance in cases where the vessel is narrow, or has an extremely large breadth. Two

vessels that may provide further insight into this assumption at each extreme are the E-Craft and the oblique icebreaker concept, respectively.

C. RESISTANCE COMPONENT SUPERPOSITION

Despite the validity of assuming truly decoupled resistance components, the models presented in literature approximate icebreaking resistance as the sum of either average or discrete values over the icebreaking cycle. If a steady state resistance value is desired at a specified velocity, the resistance components obtained from either means may be used interchangeably according to the work-energy principle.

$$V_{i+1} = \sqrt{\frac{2\Delta x}{M}\left(F_p - \sum F_{resistance}\right) + \left(V_i\right)^2} \tag{4.1}$$

In addition, these values may be interchanged to obtain a rough resistance estimate for nonlinear systems.

1. Conceptual Test

To test this concept, the Lindqvist calculation was performed for the icebreaker, Vladivostok. In the first test, it was assumed that the average value of all resistance components were present through the entire duration of the icebreaking cycle. The steady-state velocity of the icebreaker was obtained via application of the work-energy principle. In the second test, the bending resistance component was assumed to occur only upon contact with the ice sheet until failure of the ice cusp, with all cusps failing simultaneously. To further test this concept, the second test was also modified such that that individual cusps were assumed to fail at equal intervals.

a. Averaged Ice Resistance

Upon applying the work-energy method presented in Equation 4.1 to the transient numerical model, the icebreaker achieved steady-state velocity as displayed in Figure 7. This method includes the mass of the icebreaker, and therefore, more accurately represents the velocity profile of an icebreaker. In this averaged ice resistance case, all resistance values are assumed to be present at every velocity iterate. In addition, the ice resistance increases proportionally with velocity. Since the hydrodynamic resistance was not

included in this model, the increase in ice resistance causes the convergence of the velocity. In this particular case, the steady state velocity converged to approximately 0.325 m/s.

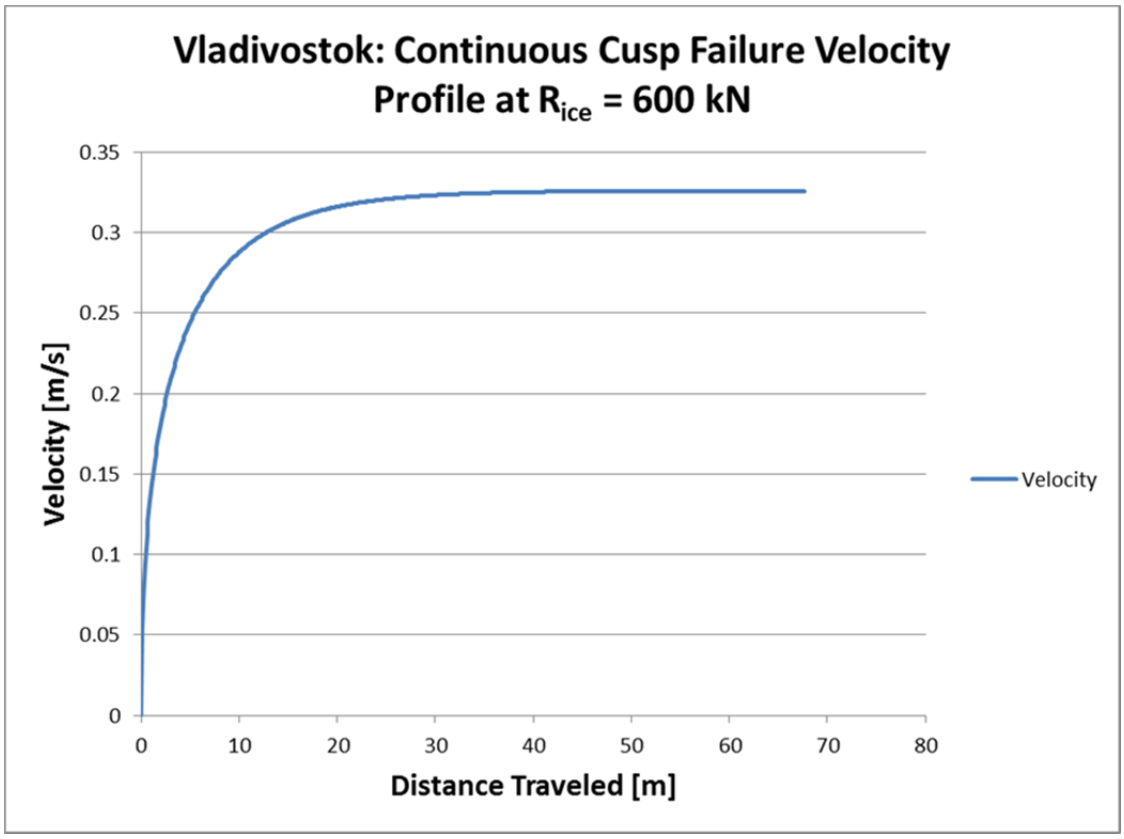

Figure 7. Continuous cusp failure transient velocity profile.

b. Cyclical Bending Resistance

The steady-state velocity profile for simultaneous and single cusp failure was obtained using Equation 4.1, appearing as a saw-tooth pattern as expected from literature [13]. Figure 8 illustrates the contrast between assuming simultaneous and individual cusp failure. This model differs from the average ice resistance model because it has the added dependence on the absolute distance traveled, along with velocity dependence. The distance traveled is significant in this model because it determines the locations of ice loading prior to cusp failure over successive icebreaking cycles. The saw-tooth velocity profile indicates nearly instantaneous momentum change of the icebreaker. When all cusps are assumed to fail simultaneously, the model may predict a lower initial

velocity limit, below which, the icebreaker is unable to proceed through the ice. Although this highlights the motivation for backing and ramming icebreaking operations, where the icebreaker cannot proceed continuously, this assumption assumes over predicts the propulsive force required to transit the ice for a given initial velocity. To provide a more realistic minimum velocity at the start of the icebreaking cycle prior to the necessitation of backing and ramming, the velocity profile resulting from the failure of a single ice cusp was maintained. This is also shown in Figure 8 as a saw-tooth velocity profile having significantly less cyclical amplitude than that predicted with the simultaneous cusp failure assumption.

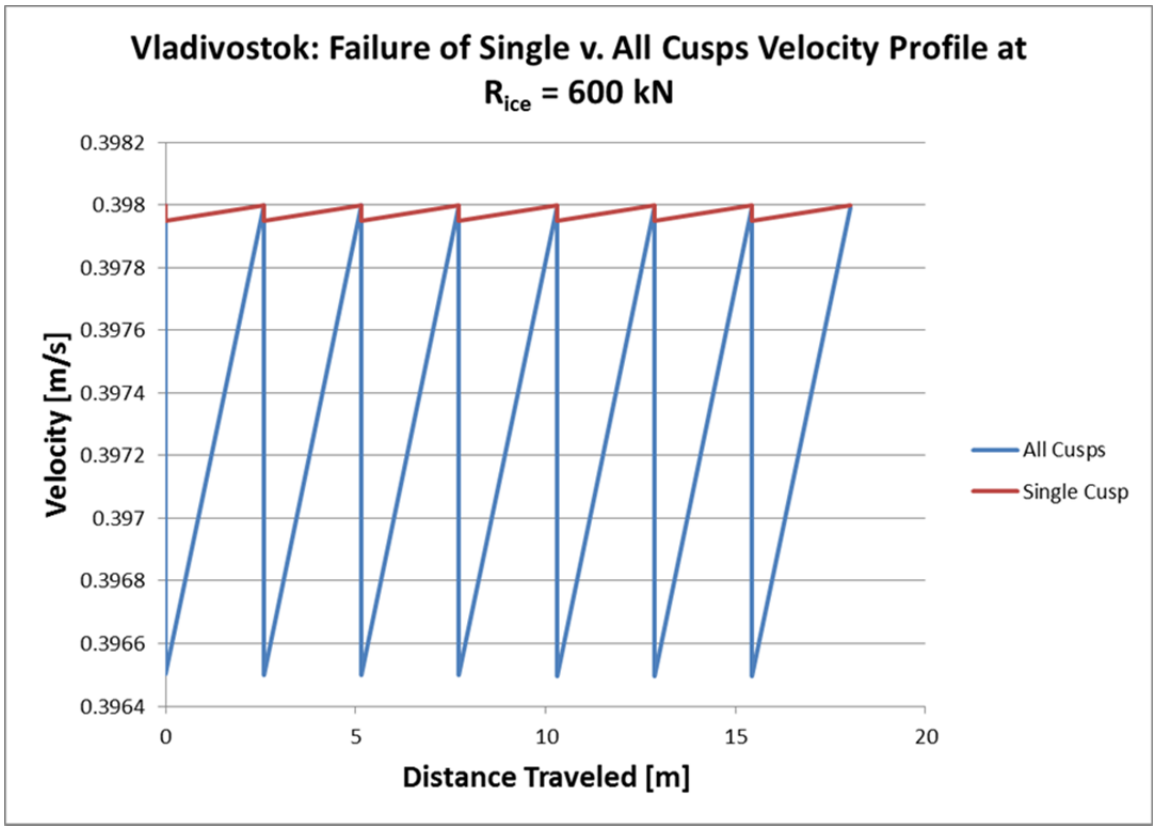

Figure 8. Cyclical cusp failure transient velocity profile.

2. Influence on Total Resistance

The steady-state velocity was converged upon for a resistance range of 534 kN, as expected for zero-velocity by the Lindqvist equation, to 1400 kN. As shown in Figure 9,

the continuous cusp failure assumption exactly overlaid the Lindqvist calculation. The cyclical cusp failure assumption, on the other hand, was unable to match neither the slope, nor the slope-intercept of the Lindqvist calculation.

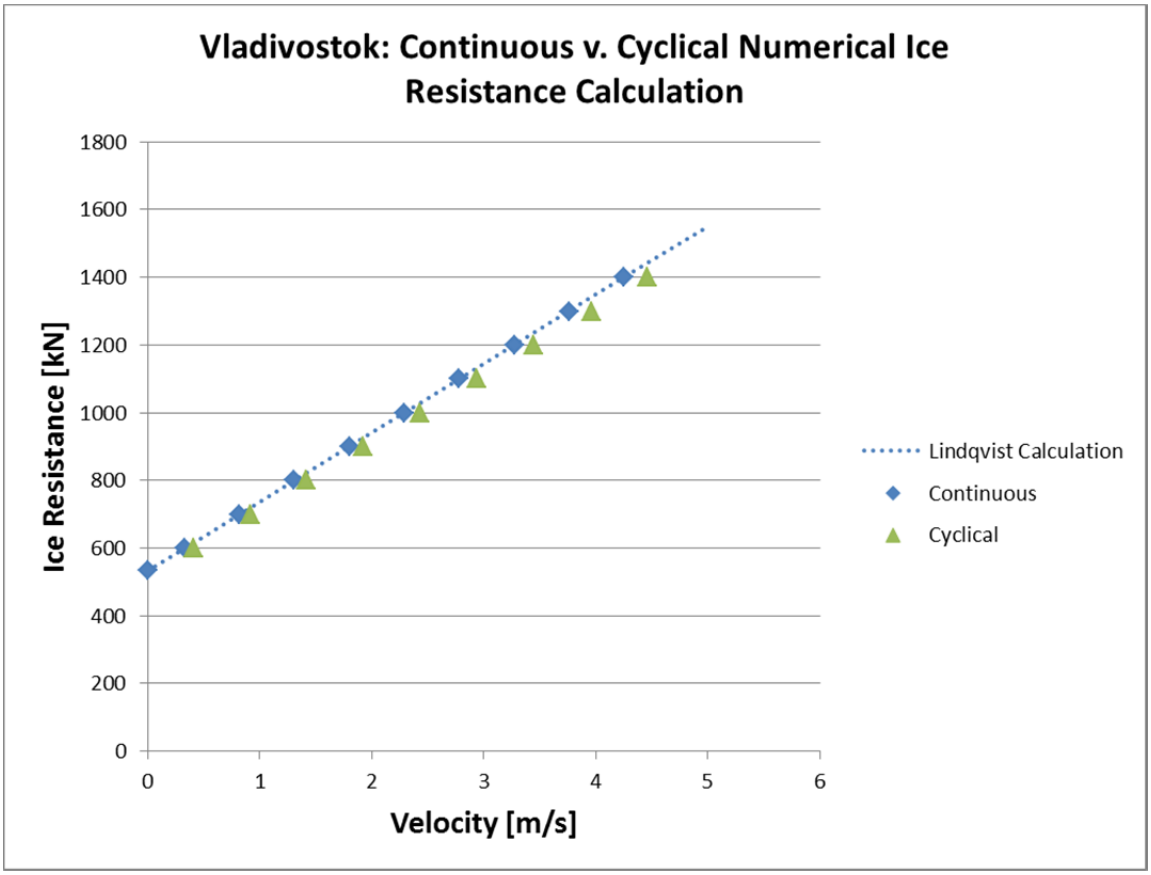

Figure 9. Comparison of continuous and cyclical cusp failure with icebreaker Vladivostok raw data and Lindqvist resistance predictions versus velocity.

The cyclical cusp failure calculation error was not expected, because this should have perfectly matched the Lindqvist calculation line. However, the average error between this numerical calculation to the values expected from the Lindqvist calculation over the resistance range was less than three percent, as shown in Figure 10. The likely cause of this error is from processing limitations. To assist this argument, the steady state velocity was obtained with a MATLAB® code included in Appendix B. Inspection of the command window output indicated that computational errors developed from calculating the square root term of the velocity iterates.

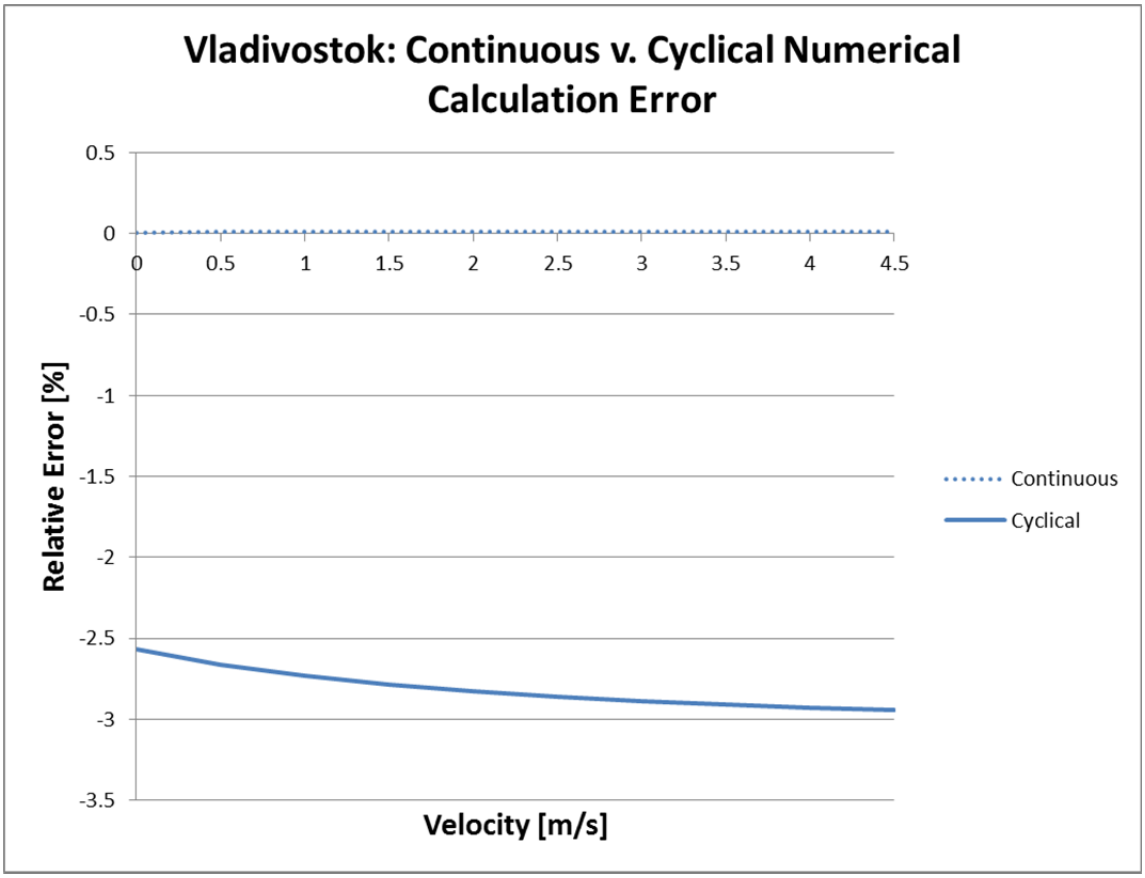

Figure 10. Comparison of continuous and cyclical cusp failure resistance-velocity relationship against icebreaker Vladivostok raw data.

D. CONCEPTUAL TEST DETERMINATION

The hybrid methodology is most easily evaluated when coupling of the resistance components is assumed negligible. By assuming zero velocity, thereby negating the rotation and hydrodynamic resistance components, the hybrid method takes a form resembling the Lindqvist method. To test the concept of multi-sourced superposition, a resistance component was obtained from a second model, and compared with the Lindqvist component. The bending resistance component was chosen for comparison since the Lindqvist approximation has a non-zero value at zero-velocity and since it is the only resistance component that is not localized to the hull-ice contact zone. Therefore, testing the resistance component has the three-fold purpose as a proof of concept for the hybrid method, cross-examination of the Lindqvist bending resistance, and to provide the ability to quantify the effects of damage to the ice analytically.

E. FINITE ELEMENT MODEL

Given the zero-velocity assumption to reduce potential analytical errors, the bending resistance was obtained from a finite element interpretation of the icebreaker providing a static distributed load to the ice sheet at the bow of the icebreaker, as shown in Figure 11.

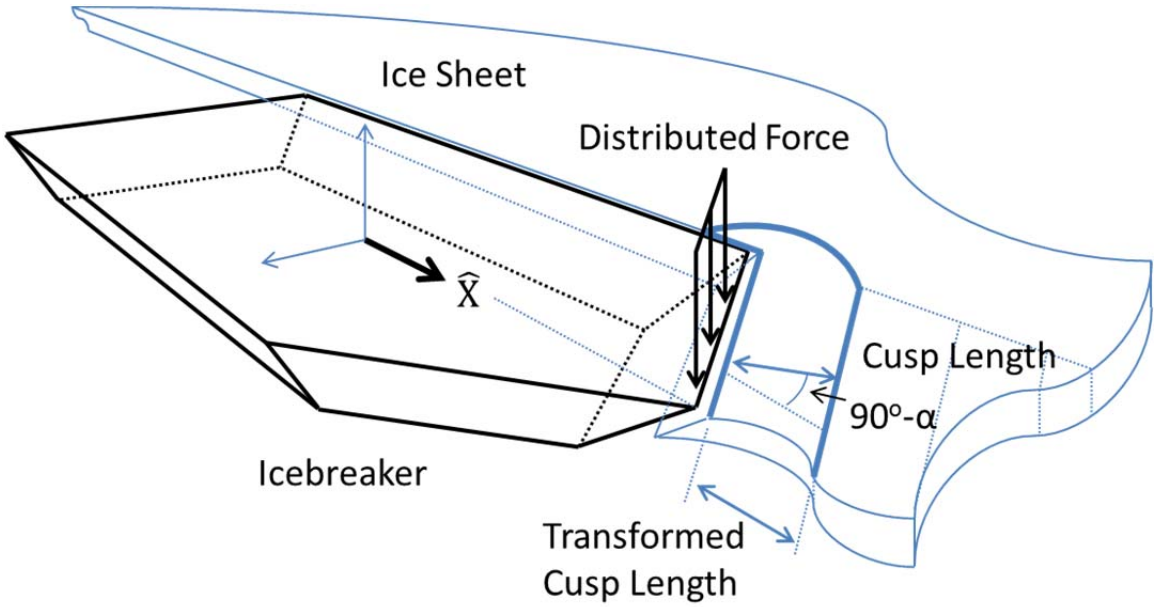

Figure 11. Illustration of ice loading, cusp length, and transformed cusp length determination in static finite-element ice bending model.

Similar to existing analytical methods, the ice sheet is assumed homogeneous and isotropic, with no spatial or time dependent properties, and supported on a uniform elastic foundation with stiffness equal to the product of sea water density and gravitational acceleration. The finite element model was generated using ANSYS Static Structural toolbox. Given the limitations of finite element modeling, it was desirable to select dimensions for the ice sheet such that the ice behaved as a semi-infinite plate consistent with prior analytical methods and that the ice had a sufficient number of nodes elements through the thickness of the ice sheet to eliminate numerical errors as the ice sheet was deformed. Assuming the icebreaking process is symmetrical about the centerline of the

icebreaker, only one half of the ice sheet was modeled to increase calculation speed. The dimensions of this half sheet of ice were arbitrarily selected as 100 m long by 35 m wide.

Ice was removed from one edge along the length of the ice sheet inwards to approximate the area occupied by the half-breadth of the icebreaker in question. In addition, this cut assumed a triangular bow form, according to the average waterline angle, to roughly approximate the influence of this parameter on the bending resistance. The ice thickness was varied through a realistic range of 0.1 m to 2.0 m. The ice sheet was bounded on the aft, forward, and outboard edges by the fixed boundary condition. The symmetric boundary condition was used along the centerline edge of the ice sheet. A uniform elastic support was applied on the underside of the ice sheet. A distributed load was applied at the hull contact area to roughly estimate the loading on the ice. To improve accuracy of the solution, mesh refinement was performed in the vicinity of the hull contact area using three-dimensional tetrahedral elements. The solution output was the bending failure stress gradient versus the distributed load acting on the ice, included as Figure 12.

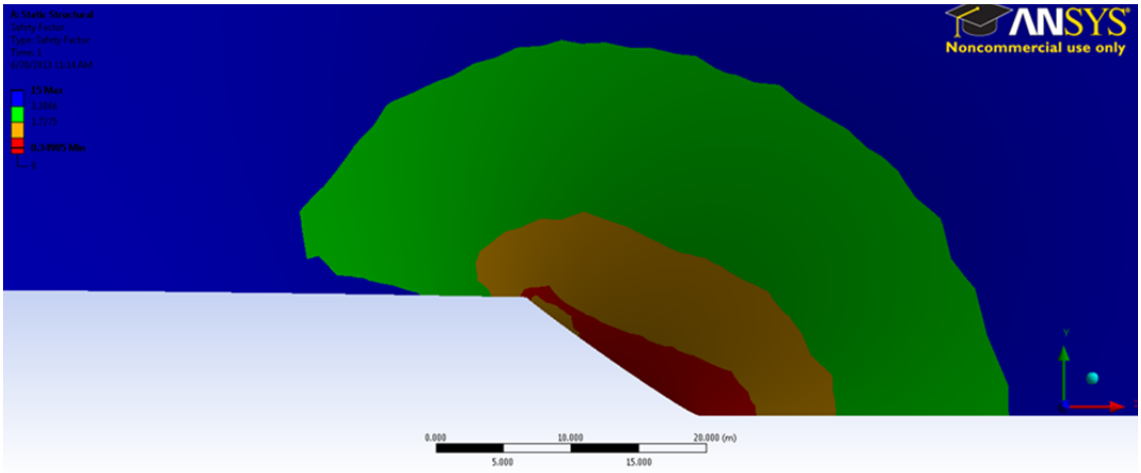

Figure 12. FEM static structural bending failure of the ice modeled in ANSYS.

The distance of ice failure ahead of the icebreaker bow was measured at multiple points with respect to the icebreaker breadth. This distance was obtained from multiple ice thicknesses and a one order magnitude range for the ice bending stress, from 0.1 MPa to 1 MPa.

F. ANALYSIS

As both the loading force and distance of broken ice ahead of the icebreaker are obtained from the finite element model, this is simply related to the existing analytical formulations for the bending resistance. Two obstacles develop, however, since analytical ice bending failure models neither represent the force as a distributed load, nor do they represent the distance ice is broken ahead of the icebreaker. The latter of the two is accounted for since it is the transformed cusp length. The implications of distributed loading, on the other hand, required further insight. As expected, without accounting for this inconsistency, the relation between the finite element and Lindqvist predictions for the bending resistance was not clear across the range of ice thicknesses. Critical observation of the Lindqvist method revealed that it assumed both cusp length and width to be equal independent of ice thickness. However, other literary sources indicated that the length and width were in fact dependent on ice thickness. Since Lindqvist approximates the bending resistance as the sum of point loads, spaced apart by the cusp width, this total resistance component is proportional to a cusp width dependent approximation. Figure 13 illustrates the load distribution and cusp failure geometry assumed as a single icebreaking cycle.

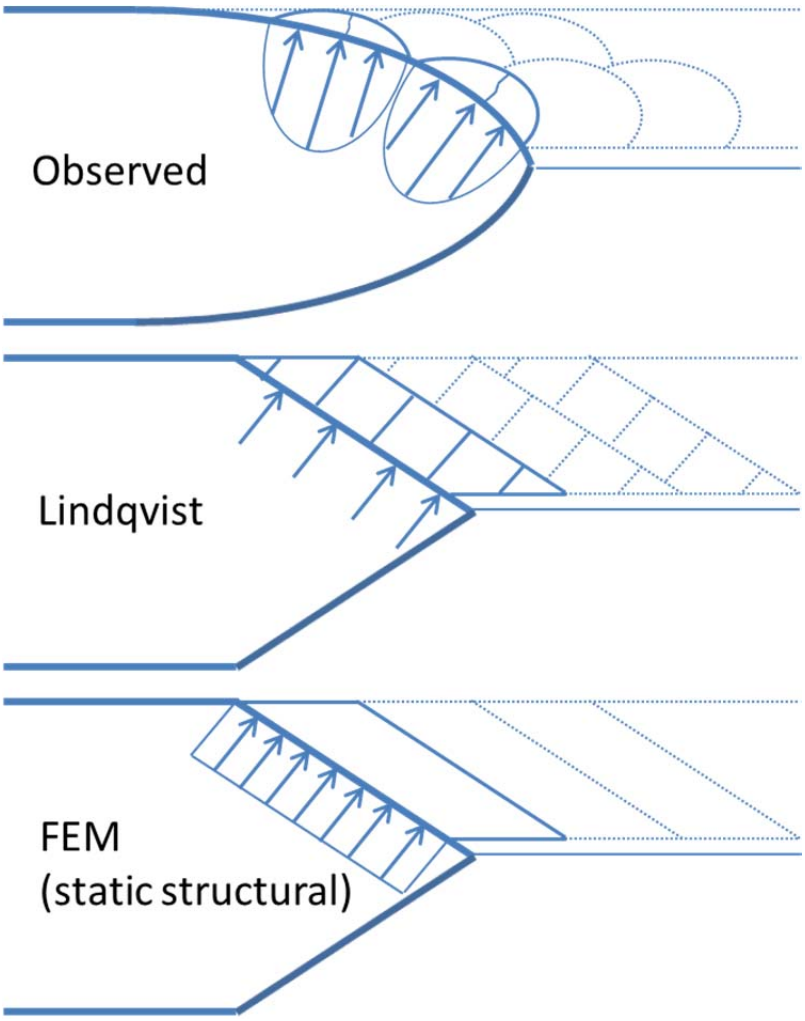

Figure 13. Illustration of ice loading and cusp failure geometry from real-world observation, the Lindqvist 2-D orthogonal ice cusp failure assumption, and the static structural finite element ice failure assumption.

Therefore, the finite element approximation for the average bending resistance force is proportional to the Lindqvist value.

$$\left[\frac{F}{l}\right]_{FEM} = A\left[\frac{F_v n}{l}\right]_{Lindqvist} \tag{4.2}$$

where A is the proportionality constant.

The average bending force predictions obtained by finite element method and Lindqvist were compared according to parameter variation through a reasonable range of values. In this comparison, the Young's modulus, bending failure stress, and thickness of

the ice, as well as the breadth of the vessel, are clearly defined in the Lindqvist equation, whereas the influence of these parameters is not clear within the finite element result. The range of parameter variation is provided in Table 7.

Table 7. Parameter variation range

Parameter	Min	Max
E	0.2 Gpa	20 Gpa
σ_b	0.1 Mpa	1.0 Mpa
H	0.1 m	2.0 m
B	10 m	30 m

Due to the enhanced ability of the finite element model to approximate the cusp failure geometry, some error was expected between the finite element and Lindqvist average force predictions. The error was linearized in all cases by multiplying the error by the variable parameter to some power. This linearization defined the proportionality constant, *A*, between the finite element and Lindqvist average force predictions. The average bending force obtained from the finite element result was then directly applied as a substitute to the Lindqvist value.

$$A = \left[1 + \left(\frac{m \cdot p + b}{100\, p^{N}}\right)\right] \tag{4.3}$$

Although this form of analysis has limitations, it generally had good agreement for the given parameters. The slope and slope-intercept of the linearized relative error was obtained and provided in Table 8.

Table 8. Parameter modification variables for proportionality constant, *A*.

p	***N***	***m***	***b***
E	0.095	4.00E-08	-602.74
σb	0.185	-0.006	-41.42
H	-0.015	40.406	-70.215
B	0.9	-69.964	968.6

All graphs in this section are presented together in Appendix C as a quick reference to this statement.

1. Young's Modulus

The Young's Modulus was varied from 0.2 GPa to 20 GPa to accommodate the wide range of values presented in literature, since this variable is expected to change significantly in the expected operating environment.

a. Uncorrected Relative Error

The relative error between the average bending force obtained via the finite element and Lindqvist models are provided in Figure 14, showing nonlinear dependence on parameter variation.

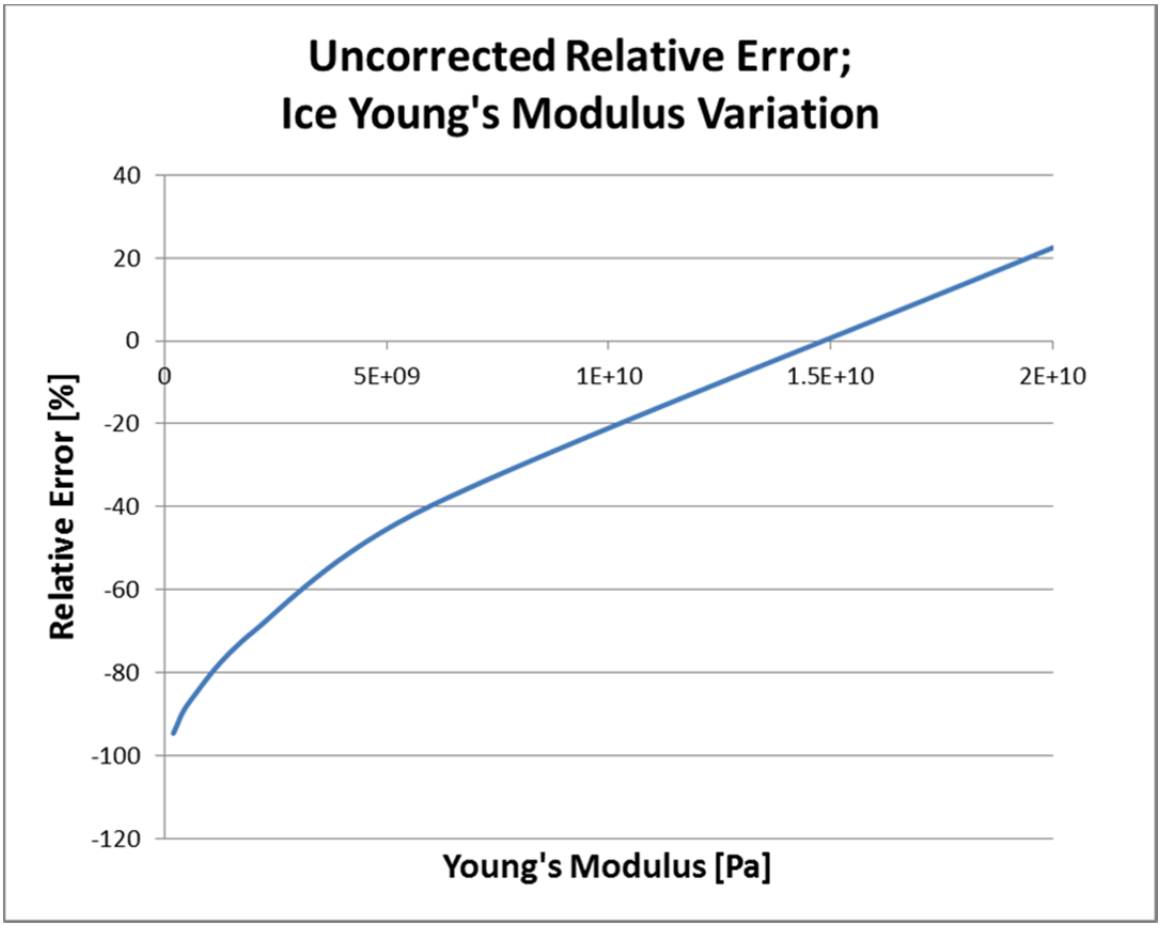

Figure 14. Uncorrected relative error of the finite element average bending force v. Lindqvist when varying the ice Young's modulus.

b. Linearized Relative Error

The data was linearized by multiplying the error by the Young's modulus to the power of 0.095, producing a best fit line with an R^2 value of 0.998, as shown in Figure 15.

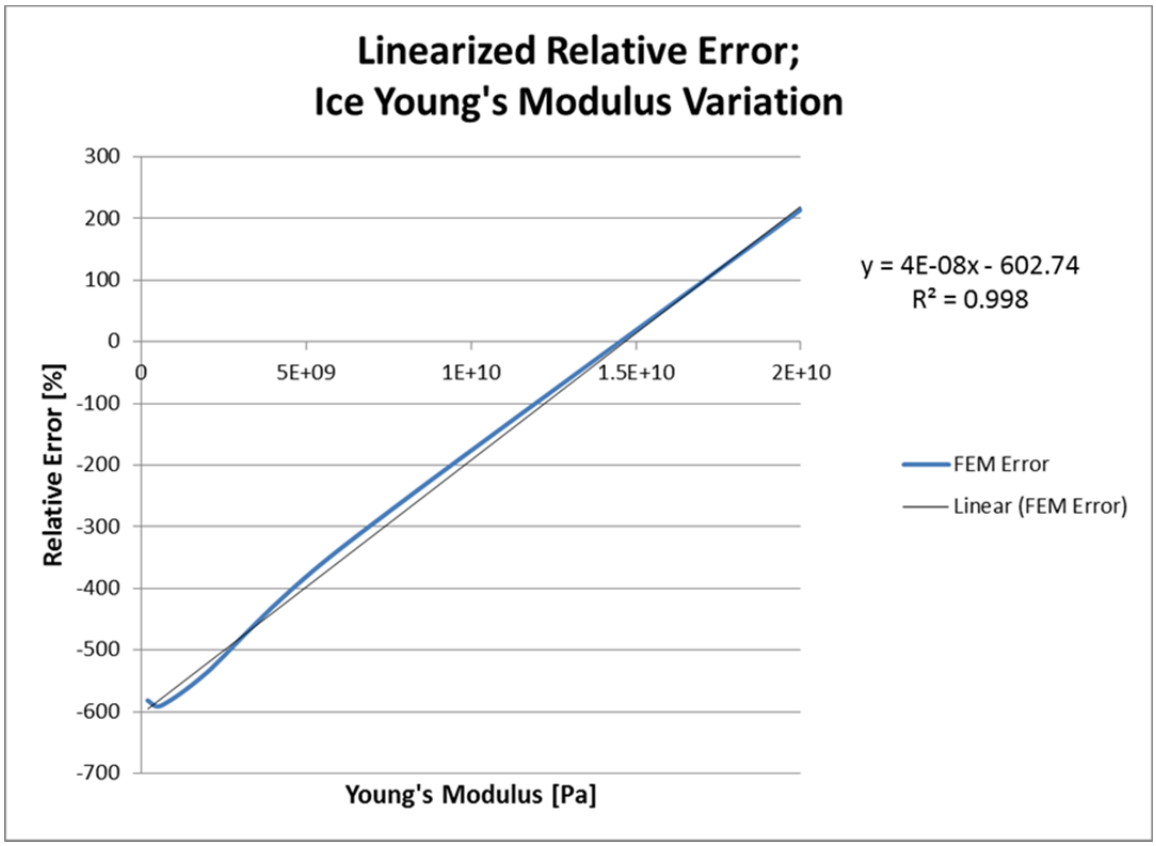

Figure 15. Linearized relative error of the finite element average bending force v. Lindqvist when varying the ice Young's modulus.

c. Corrected Average Bending Force

The best fit error prediction line was then used to correct the finite element prediction to the Lindqvist value according to Equation 4.3. The corrected average bending force obtained by finite element method is compared with the Lindqvist prediction in Figure 16. The data sets are consistent, as expected from this analysis. However, the slope-intercept of the finite element corrected value appears to be significantly greater than that predicted by Lindqvist. Since the average bending force

curves are nearly vertical as the Young's modulus approaches zero, this error was expected by numerical processing limitations.

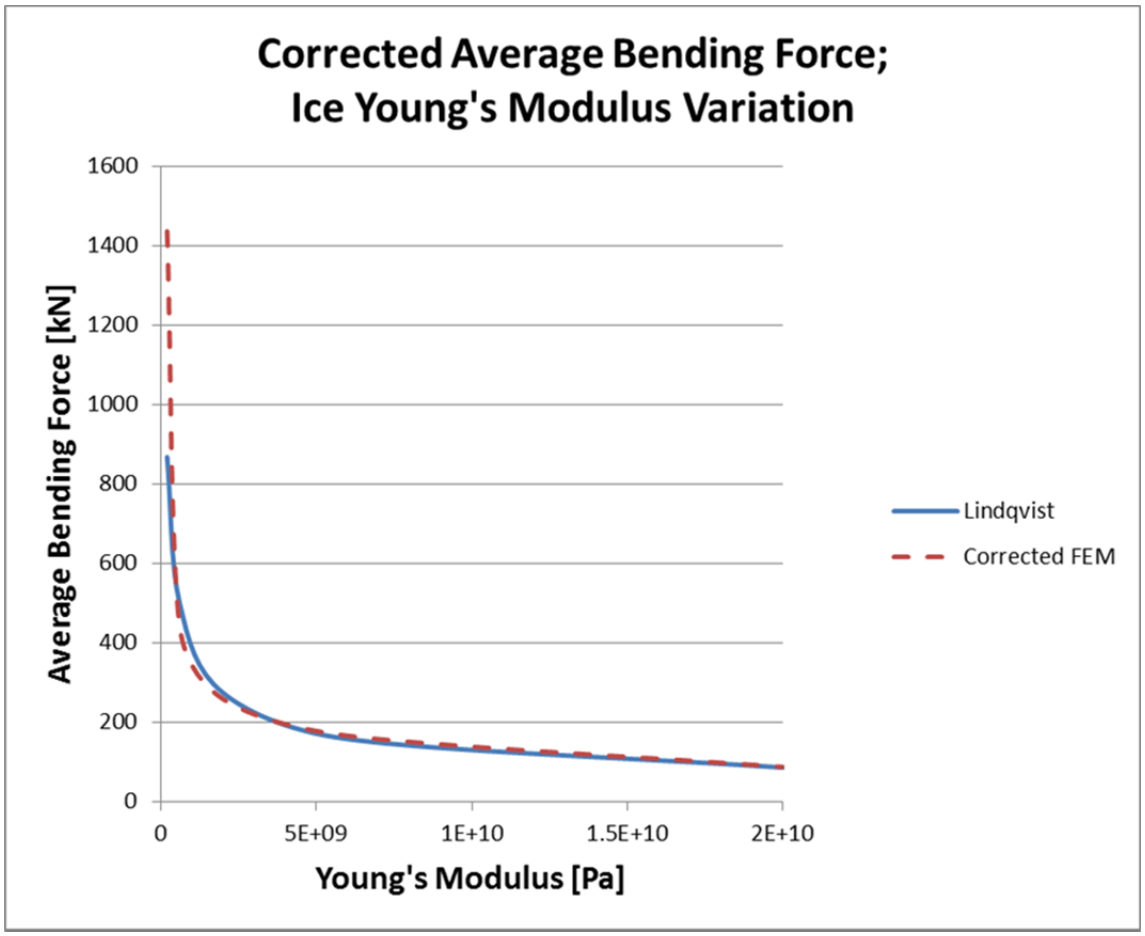

Figure 16. Corrected finite element average bending force v. Lindqvist when varying the ice Young's modulus.

d. Corrected Relative Error

To finalize the parameter variation of Young's modulus, the relative error of the corrected finite element prediction for the average bending force was compared with the Lindqvist value, as shown in Figure 17. As stated before, significant errors were expected as the Young's modulus approached zero. However, if this region is neglected, the finite element obtained force nearly matches the Lindqvist prediction with a maximum error of 11.3% and a minimum of 1.5%.

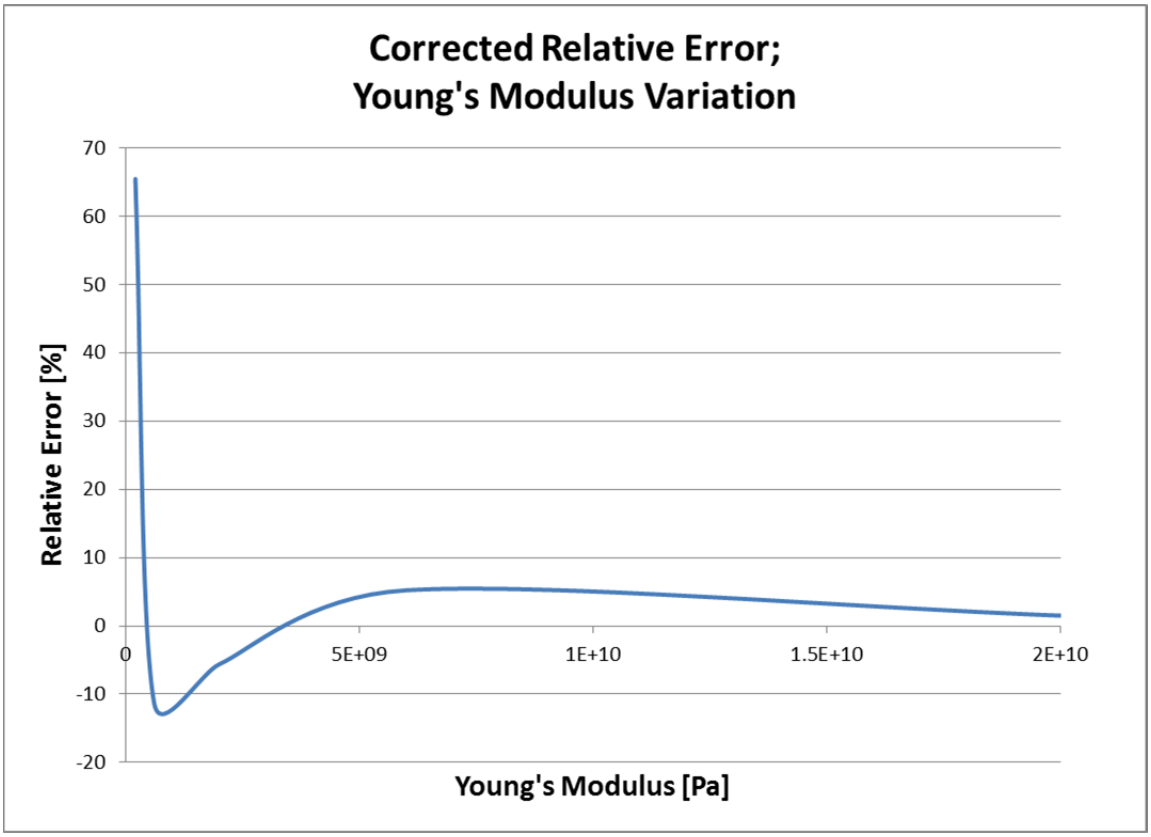

Figure 17. Corrected relative error of the finite element average bending force v. Lindqvist when varying the ice Young's modulus.

2. Bending Failure Stress

The error between the Lindqvist and finite element average bending force predictions was obtained for the bending stress range of 0.1 MPa to 1 MPa to be consistent with the range of values obtained during in-situ measurement.

a. Uncorrected Relative Error

The relative error between the average bending force obtained via the finite element and Lindqvist models are provided in Figure 18, showing nonlinear dependence on parameter variation.

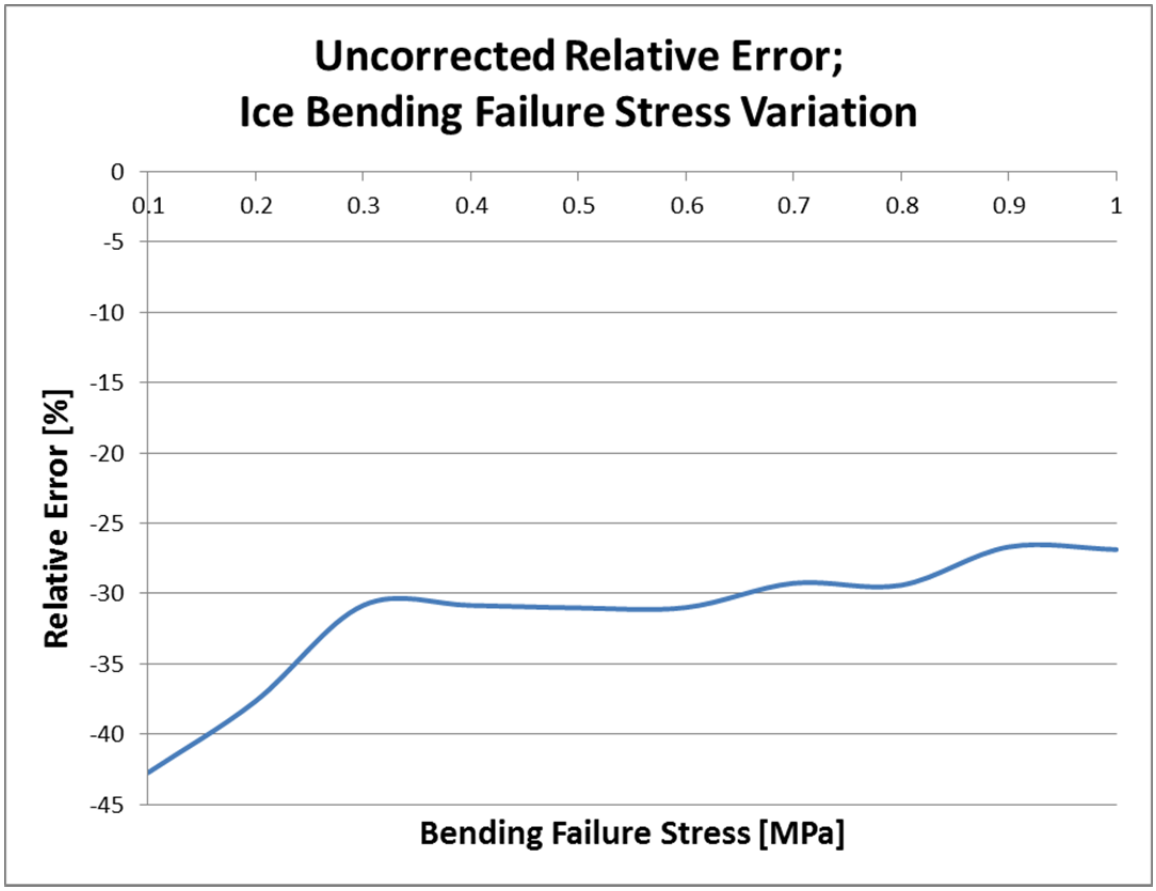

Figure 18. Uncorrected relative error of the finite element average bending force v. Lindqvist when varying the ice bending failure stress.

b. Linearized Relative Error

The data was linearized by multiplying the error by the bending failure stress to the power of 0.185, producing a best fit line with reasonable agreement to the errors presented, as shown in Figure 19.

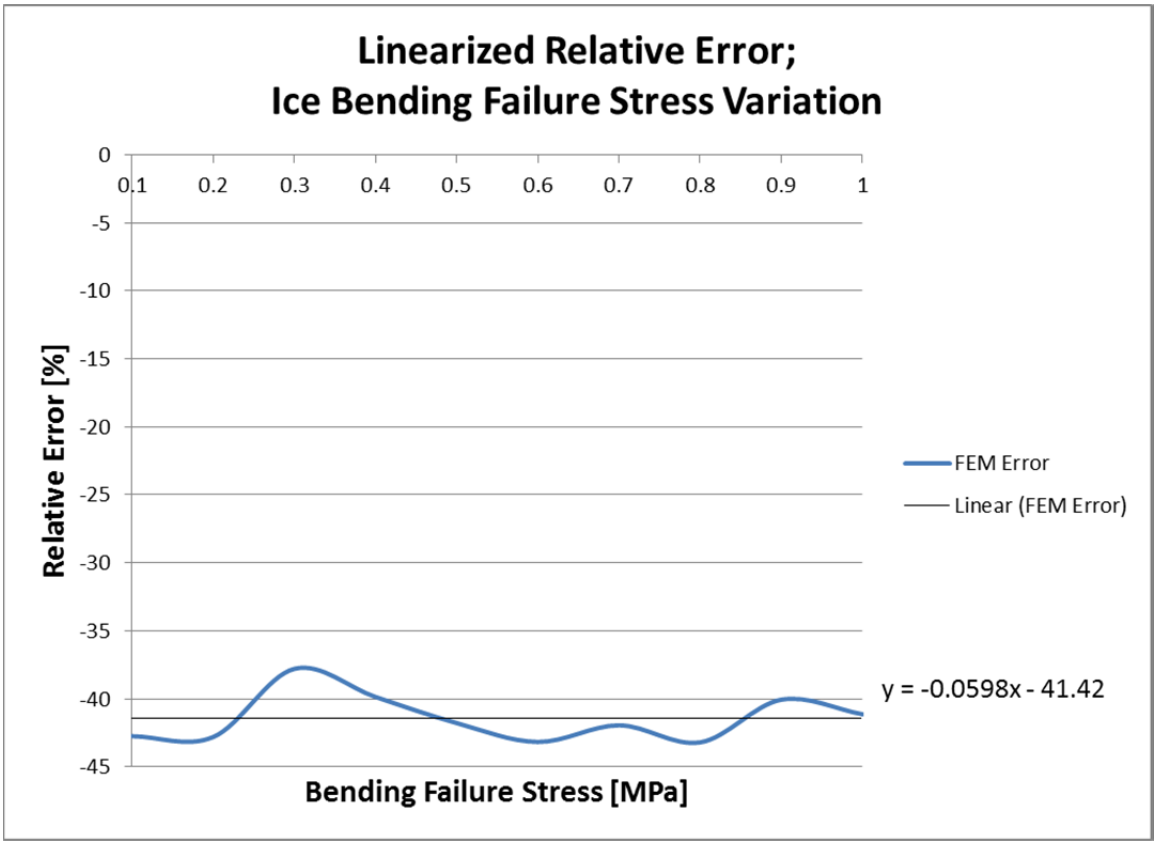

Figure 19. Linearized relative error of the finite element average bending force v. Lindqvist when varying the ice bending failure stress.

c. Corrected Average Bending Force

The best fit error prediction line was then used to correct the finite element prediction to the Lindqvist value according to Equation 4.3. The corrected average bending force obtained by finite element method is compared with the Lindqvist prediction in Figure 20. The data sets are consistent, as expected from this analysis.

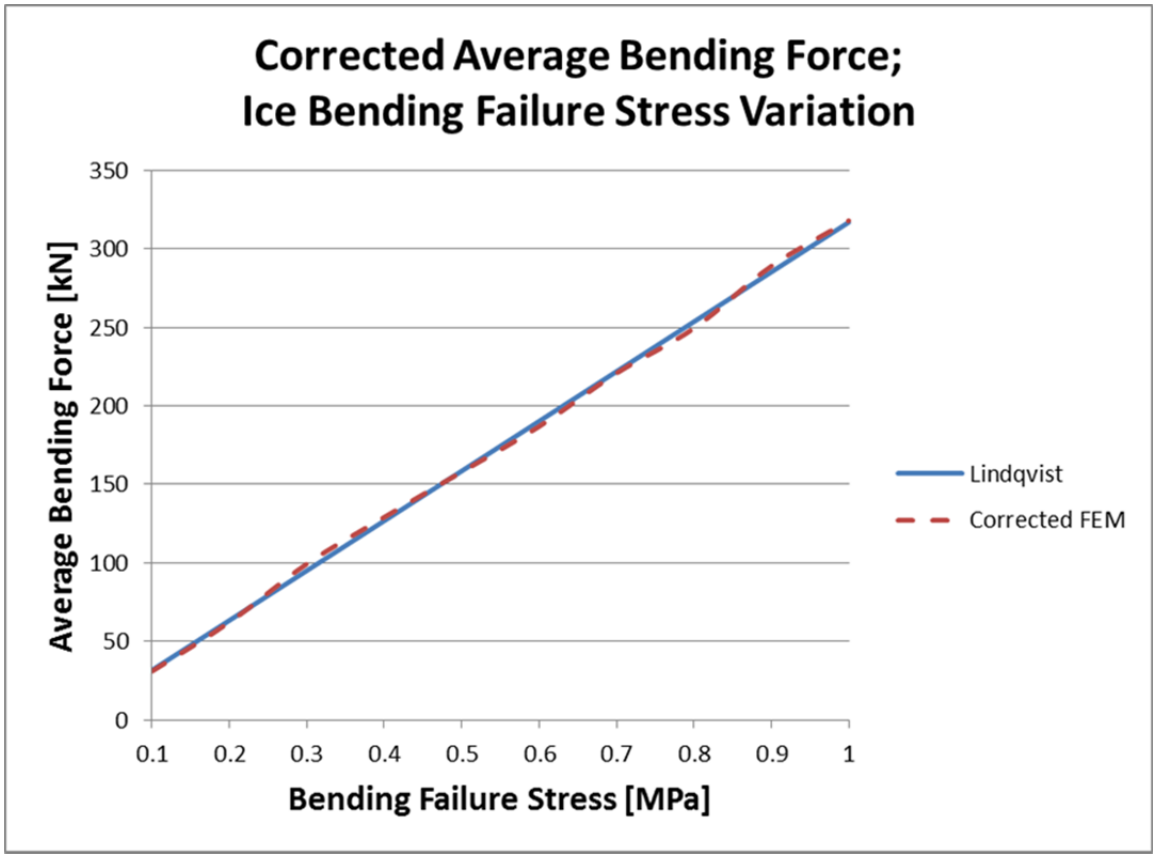

Figure 20. Corrected finite element average bending force v. Lindqvist when varying the bending ice failure stress.

d. Corrected Relative Error

To finalize the parameter variation of the bending failure stress, the relative error of the corrected finite element prediction for the average bending force was compared with the Lindqvist value, as shown in Figure 21. Although the error curve is nonlinear, the maximum and minimum errors are 2.3% and 0.3%, respectively.

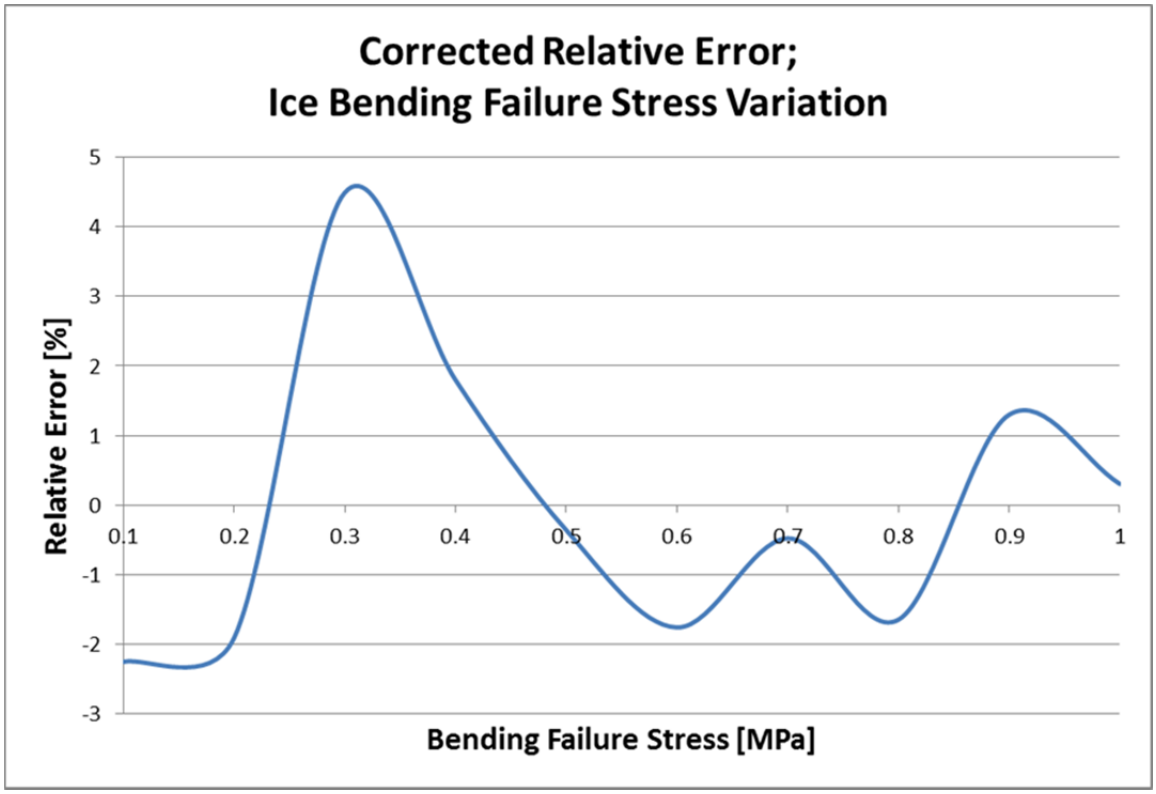

Figure 21. Corrected relative error of the finite element average bending force v. Lindqvist when varying the ice bending failure stress.

3. Ice Thickness

The error between the Lindqvist and finite element average bending force predictions was obtained for ice thickness ranging from 0.1 m to 2.0 m. This variable is expected to change significantly in the expected operating environment.

a. Uncorrected Relative Error

The relative error between the average bending force obtained via the finite element and Lindqvist models are provided in Figure 22, showing limited if any dependence on parameter variation.

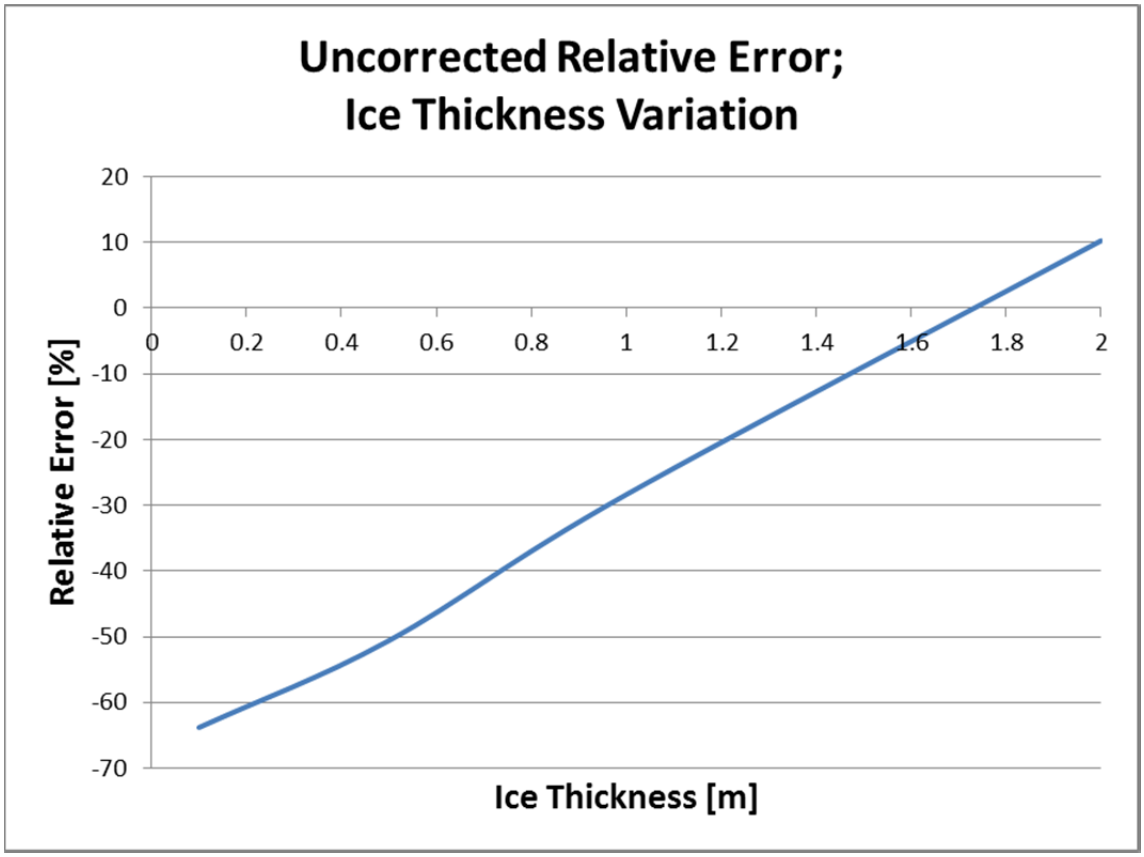

Figure 22. Uncorrected relative error of the finite element average bending force v. Lindqvist when varying the ice thickness.

b. Linearized Relative Error

Although the prediction appears to fit well without correction, the data was linearized by multiplying the error by the bending failure stress to the power of -0.015, producing a best fit line which mitigated residual errors, as shown in Figure 23.

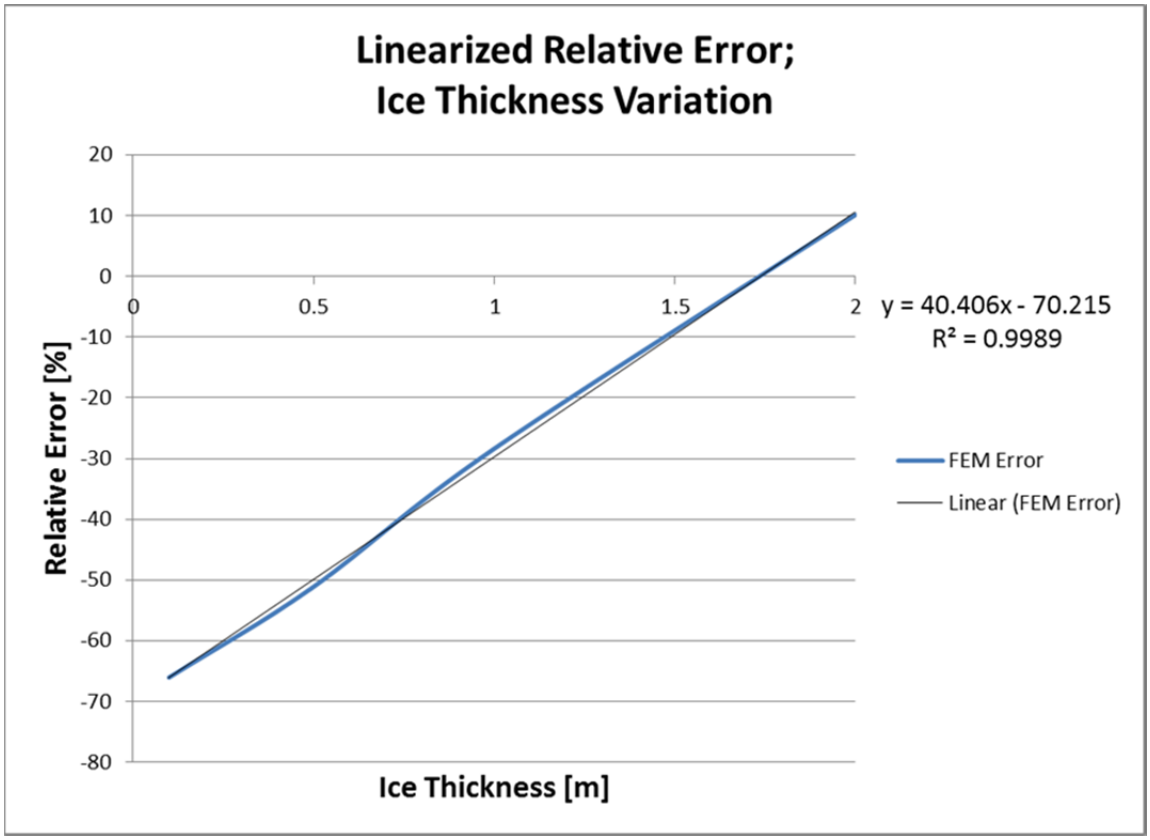

Figure 23. Linearized relative error of the finite element average bending force v. Lindqvist when varying the ice thickness.

c. Corrected Average Bending Force

The best fit error prediction line was then used to correct the finite element prediction to the Lindqvist value according to Equation 4.3. The corrected average bending force obtained by finite element method is compared with the Lindqvist prediction in Figure 24. The data sets are consistent, as expected from this analysis.

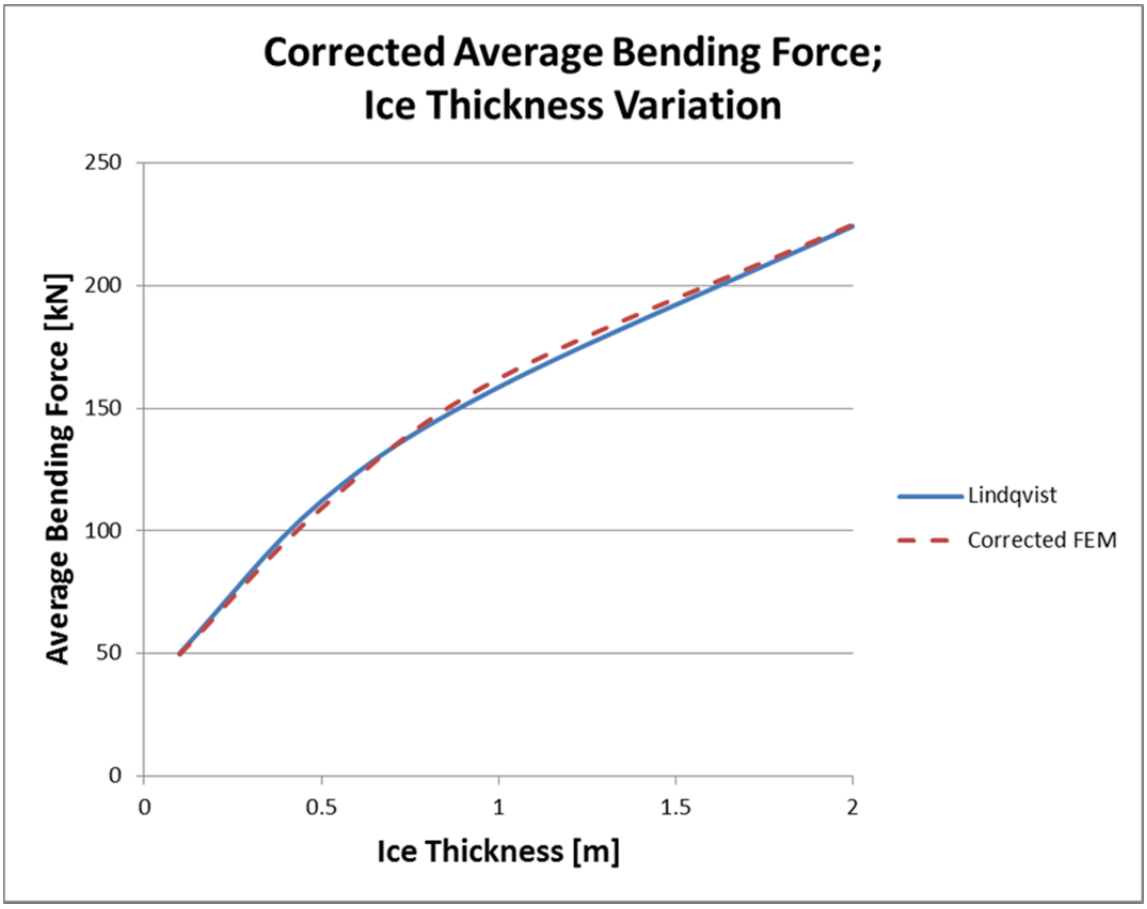

Figure 24. Corrected finite element average bending force v. Lindqvist when varying the ice thickness.

d. Corrected Relative Error

To finalize the parameter variation of the ice thickness, the relative error of the corrected finite element prediction for the average bending force was compared with the Lindqvist value, as shown in Figure 25. Despite the curve presented in the error plot, the maximum and minimum errors were 1.0% and 0.3%, respectively.

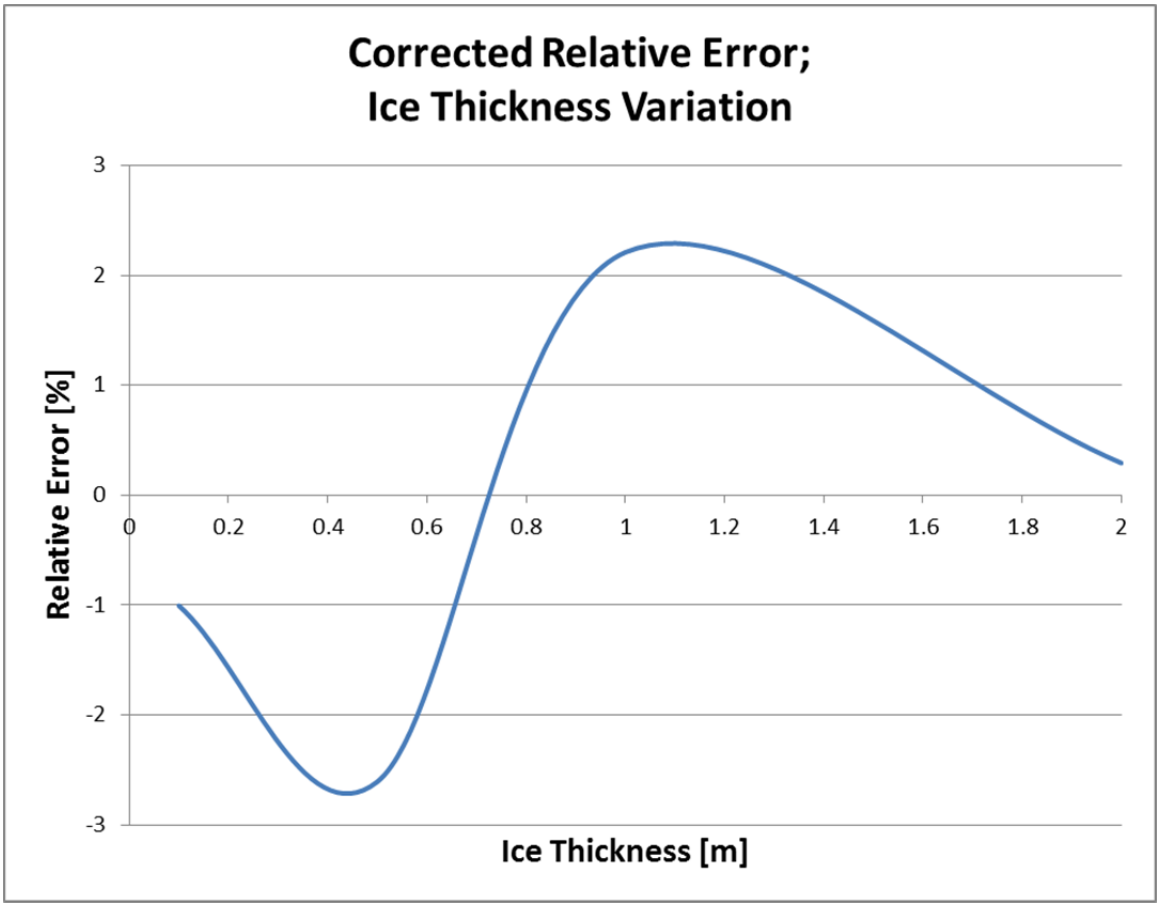

Figure 25. Corrected relative error of the finite element average bending force v. Lindqvist when varying the ice thickness.

4. Vessel Breadth

The error between the Lindqvist and finite element average bending force predictions was obtained for vessel breadth in the range of 10 m to 30 m, consistent with most icebreaking vessels.

a. Uncorrected Relative Error

The relative error between the average bending force obtained via the finite element and Lindqvist models are provided in Figure 26, showing nonlinear dependence on parameter variation.

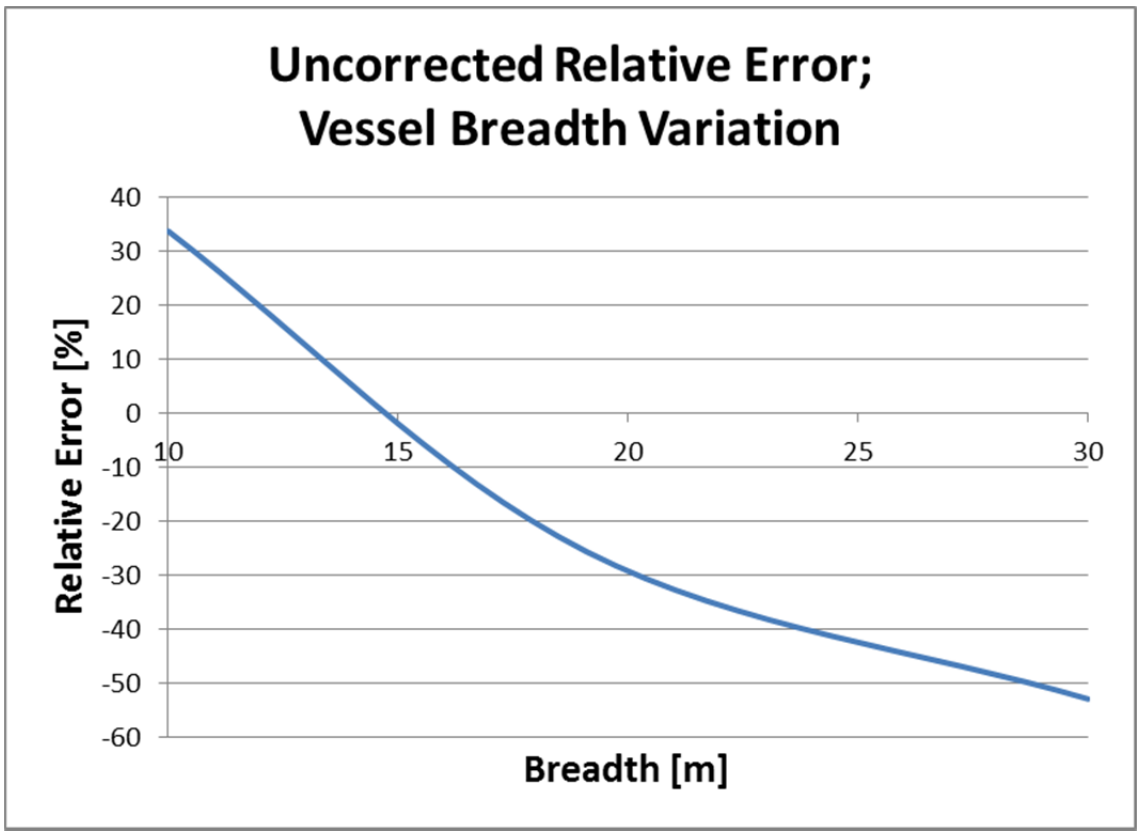

Figure 26. Uncorrected relative error of the finite element average bending force v. Lindqvist when varying the vessel breadth.

b. Linearized Relative Error

The data was linearized by multiplying the error by the bending failure stress to the power of 0.9, producing a best fit line with reasonable agreement to the errors presented, as shown in Figure 27.

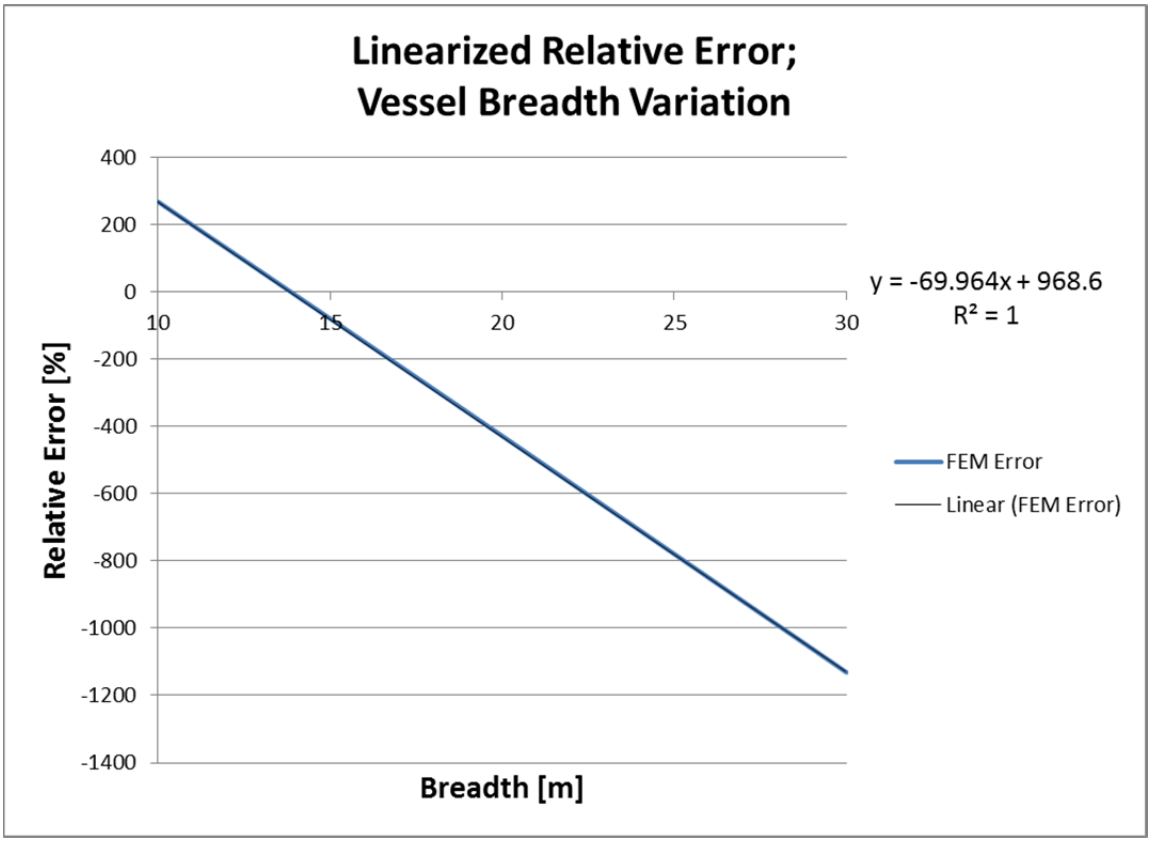

Figure 27. Linearized relative error of the finite element average bending force v. Lindqvist when varying the vessel breadth.

c. Corrected Average Bending Force

The best fit error prediction line was then used to correct the finite element prediction to the Lindqvist value according to Equation 4.3. The corrected average bending force obtained by finite element method is compared with the Lindqvist prediction in Figure 28. The data sets are consistent, as expected from this analysis.

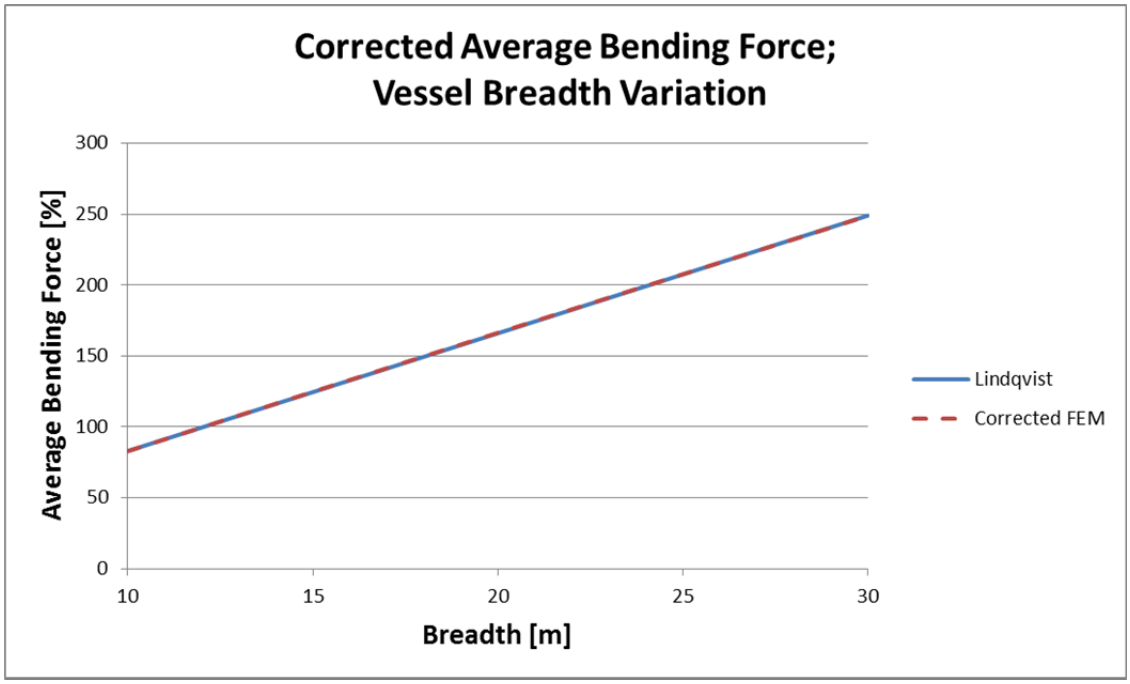

Figure 28. Corrected finite element average bending force v. Lindqvist when varying the vessel breadth.

d. Corrected Relative Error

To finalize the parameter variation of vessel breadth, the relative error of the corrected finite element prediction for the average bending force was compared with the Lindqvist value, as shown in Figure 29. Despite the curve presented in the error plot, the maximum error was 0.11% and the minimum error was 0.09%.

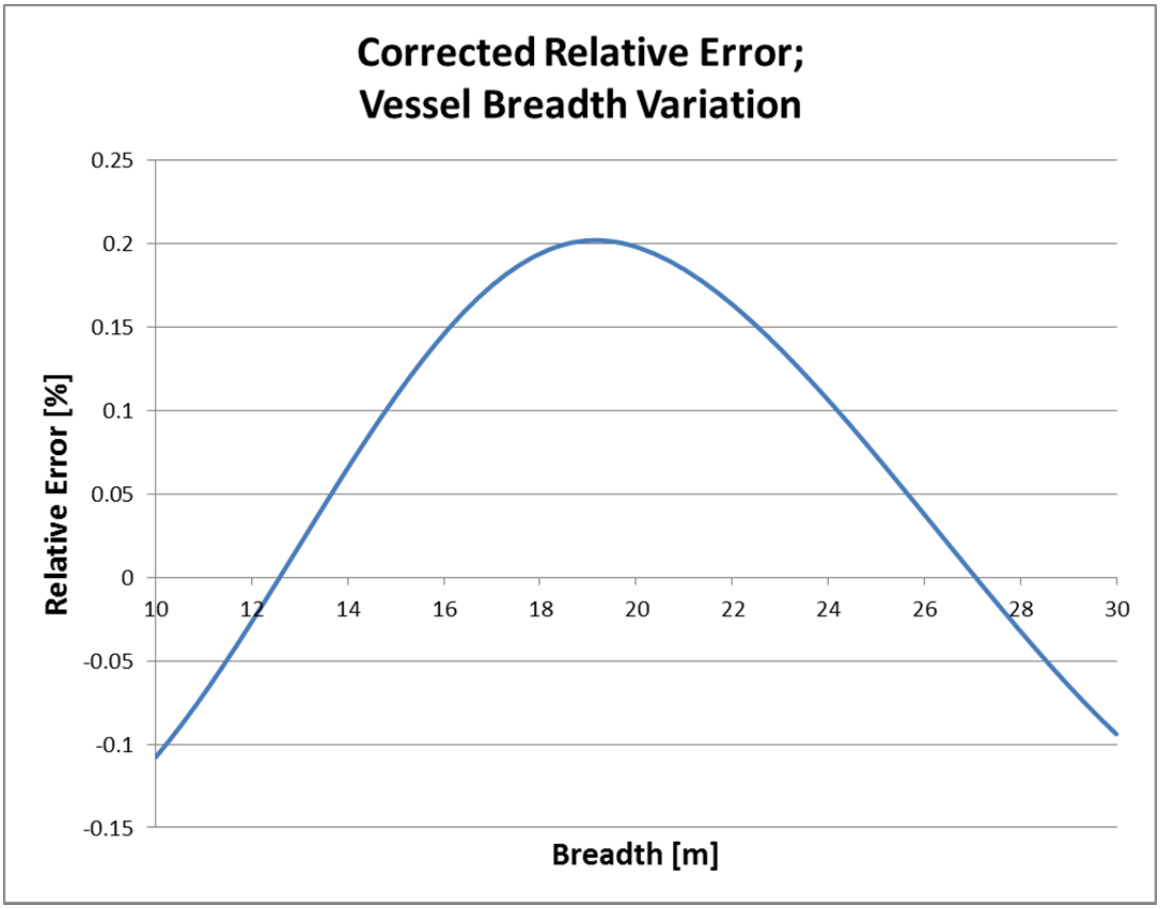

Figure 29. Corrected relative error of the finite element average bending force v. Lindqvist when varying the ice vessel breadth

V. DAMAGED ICE SHEET RESISTANCE PREDICTION

A. TEST SPECIFICATION

Following the development of the hybrid bending resistance calculation, the finite element model of the ice sheet was altered to represent specific damage patterns prior to interaction with the icebreaker hull. This modified ice sheet was then loaded with the icebreaker hull, and this load was substituted for the analytical bending resistance component in the Lindqvist calculation. As the substitution errors are relatively small for the range of values selected in this initial study, the variation in total ice resistance resulting from the damage to the ice sheet contains minimal error within the limitations of the static structural finite element model. Although there are infinite ice damaging strategies that may be implemented, this study only entertains the concept of linear cuts travelling parallel to the icebreaker at three locations along the breadth of the vessel; at the vessel centerline, at 1m outboard of the extreme breadth, and 2m outboard of the extreme breadth. The cuts were defined as either partial penetration through 50% of the ice sheet, or as full penetration cuts and were assumed to occur at some distance well ahead of the icebreaker. In total, 8 specific damage patterns were tested. The tests are identified in Table 9.

Table 9. Ice damage test case identification

Test Case	Location	Depth
1	Side [1m]	50%
2	Side [1m]	100%
3	Side [2m]	50%
4	Side [2m]	100%
5	Center	50%
6	Center	100%
7	Side [1m] and Center	50%
8	Side [1m] and Center	100%

B. RESULTS

The ice was damaged according to the patterns defined in the test specification, and this was accounted for as an averaged bending force. The finite element bending failure stress contours are included in this section to illustrate the location of damage and the expected failure regions. The obtained bending resistance component for damaged ice relative to undamaged ice is included in Table 10.

Table 10. Relative bending resistance of undamaged ice versus damaged ice by test case.

Test Case	Location	Depth	Rb [%]
1	Side [1m]	50%	132.40
2	Side [1m]	100%	11.16
3	Side [2m]	50%	119.54
4	Side [2m]	100%	147.52
5	Center	50%	159.23
6	Center	100%	24.63
7	Side [1m] and Center	50%	68.17
8	Side [1m] and Center	100%	6.00

1. Side Cut [1m]

This cut involves a cut 1m outboard of the extreme breadth of the icebreaker, running parallel to the vessel's longitudinal dimension in the finite element model.

a. Partial

The cut was initiated at the upper surface of the ice through 50% of its thickness. The ice directly ahead of the icebreaker failed similarly to the undamaged ice model; however, the stress contour is visible at the cut location. The finite element solution to this damage pattern for the bending failure stress contour is included as Figure 30.

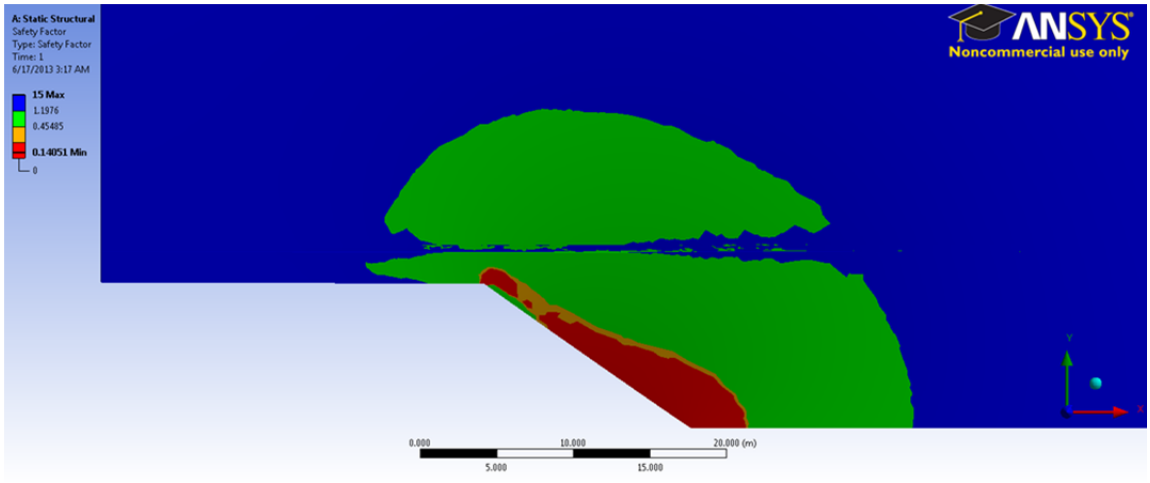

Figure 30. Bending failure stress contour for a partial side cut located 1m outboard of the extreme breadth of the icebreaker.

b. Full

The cut was initiated at the upper surface of the ice through the entire thickness, constituting the removal of the entire thickness of the ice at the location of the cut. The ice failure region differs considerably from the undamaged ice model, indicating stress concentrations at both the forward most extent of the cut and at the icebreaker shoulder. The finite element solution to this damage pattern for the bending failure stress contour is included as Figure 31.

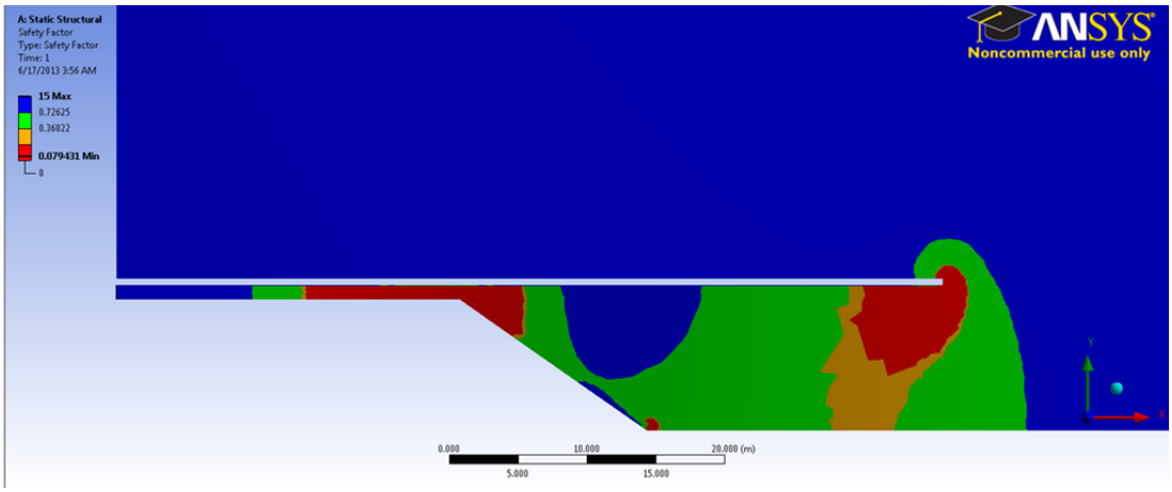

Figure 31. Bending failure stress contour for a full penetration side cut located 1m outboard of the extreme breadth of the icebreaker.

2. Side Cut [2m]

This cut involves a cut 2m outboard of the extreme breadth of the icebreaker, running parallel to the vessel's longitudinal dimension in the finite element model.

a. Partial

The cut was initiated at the upper surface of the ice through 50% of its thickness. The ice directly ahead of the icebreaker failed similarly to the undamaged ice model, however, the stress contour is visible at the cut location. The finite element solution to this damage pattern for the bending failure stress contour is included as Figure 32.

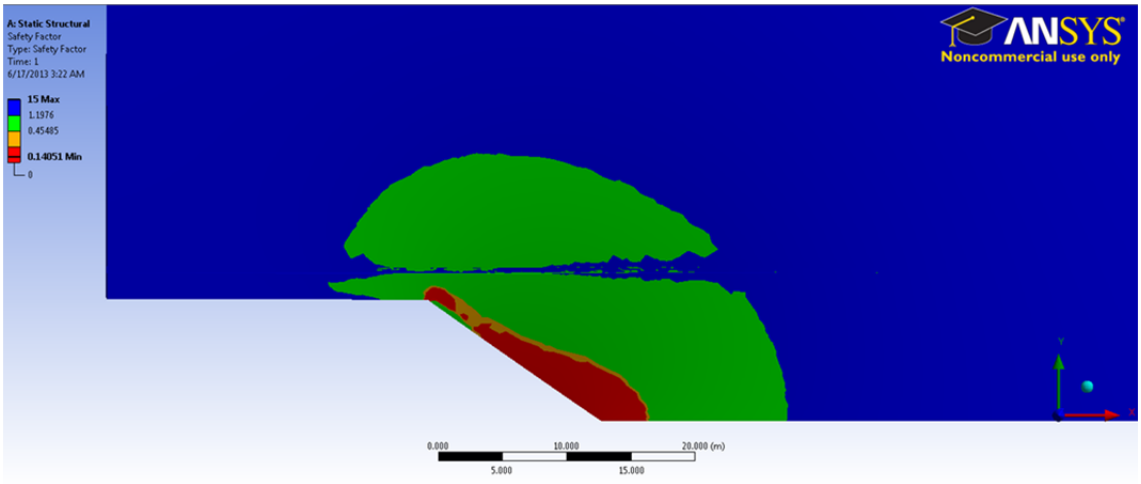

Figure 32. Bending failure stress contour for a partial side cut located 2m outboard of the extreme breadth of the icebreaker.

b. Full

The cut was initiated at the upper surface of the ice through the entire thickness, constituting the removal of the entire thickness of the ice at the location of the cut. The ice failure region differs considerably from the undamaged ice model, indicating stress concentrations at both the forward most extent of the cut and at the icebreaker shoulder. The finite element solution to this damage pattern for the bending failure stress contour is included as Figure 33.

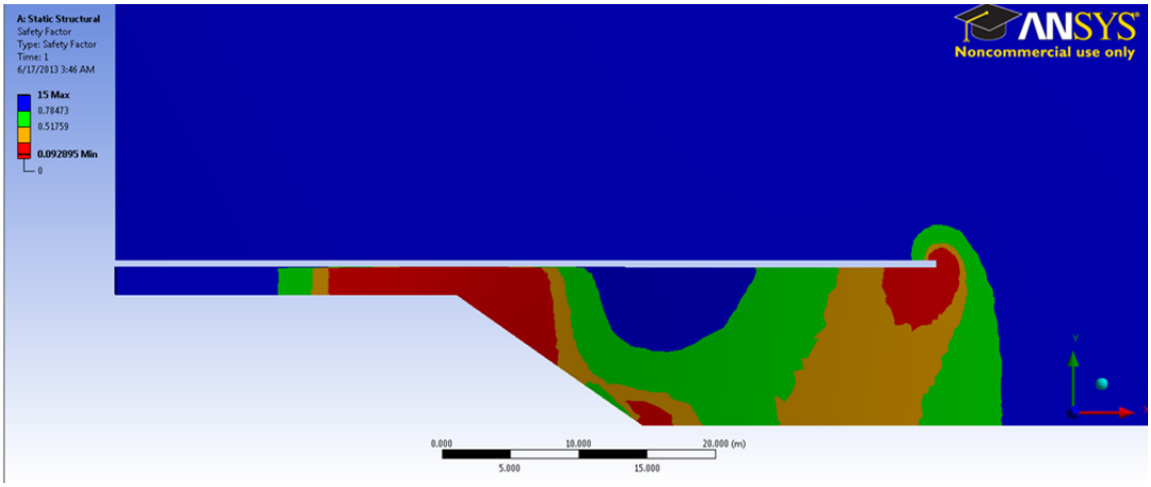

Figure 33. Bending failure stress contour for a full penetration side cut located 2m outboard of the extreme breadth of the icebreaker.

3. Center Cut

This cut involves a cut at the centerline of the icebreaker, and running parallel to the vessel's longitudinal dimension in the finite element model.

a. Partial

The cut was initiated at the upper surface of the ice through 50% of its thickness. The ice directly ahead of the icebreaker failed similarly to the undamaged ice model, however, a high stress region extends forward of the stem of the icebreaker at the cut location. The finite element solution to this damage pattern for the bending failure stress contour is included as Figure 34.

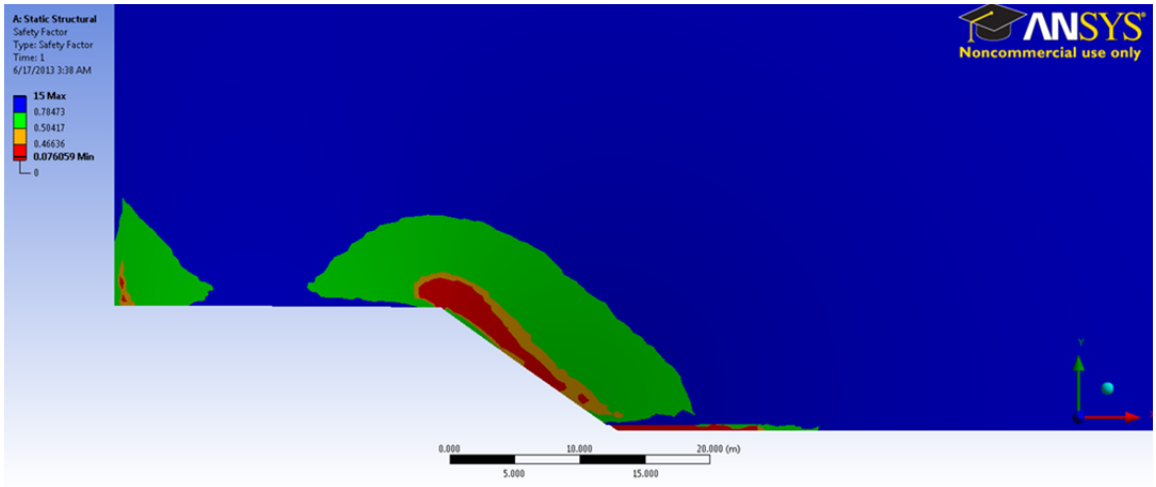

Figure 34. Bending failure stress contour for a partial penetration centerline cut located at the stem of the icebreaker.

b. Full

The cut was initiated at the upper surface of the ice through the entire thickness, constituting the removal of the entire thickness of the ice at the location of the cut. The ice directly ahead of the icebreaker failed similarly to the undamaged ice model; however stress concentrations occurred at both the forward most extent of the cut and at the icebreaker shoulder. The finite element solution to this damage pattern for the bending failure stress contour is included as Figure 35.

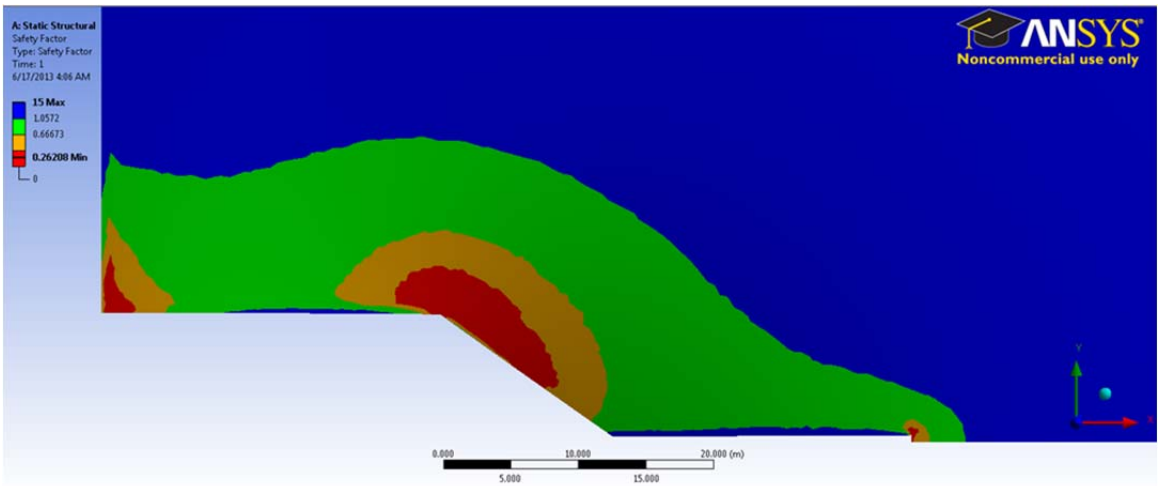

Figure 35. Bending failure stress contour for a full penetration centerline cut located at the stem of the icebreaker.

4. Side and Center Cut

This cut involves both a cut 1m outboard of the extreme breadth of the icebreaker and at its centerline, running parallel to the vessel's longitudinal dimension in the finite element model.

a. Partial

The cut was initiated at the upper surface of the ice through 50% of its thickness. The ice directly ahead of the icebreaker failed similarly to the undamaged ice model; however, high stress regions develop at the shoulders and directly forward of the stem of the icebreaker at the cut locations. The finite element solution to this damage pattern for the bending failure stress contour is included as Figure 36.

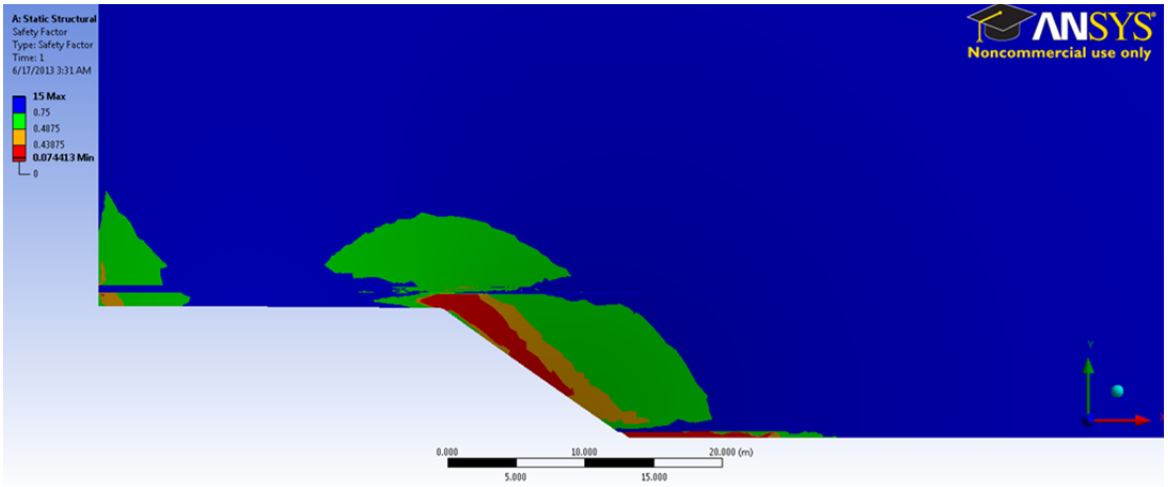

Figure 36. Bending failure stress contour for partial penetration side and centerline cuts, located at the extreme breadth and stem of the icebreaker, respectively.

b. Full

The cut was initiated at the upper surface of the ice through the entire thickness, constituting the removal of the entire thickness of the ice at the location of the cuts. The ice failure region differs considerably from the undamaged ice model; indicating stress concentrations at both the forward most extent of the cut and at the icebreaker shoulder. The finite element solution to this damage pattern for the bending failure stress contour is included as Figure 37.

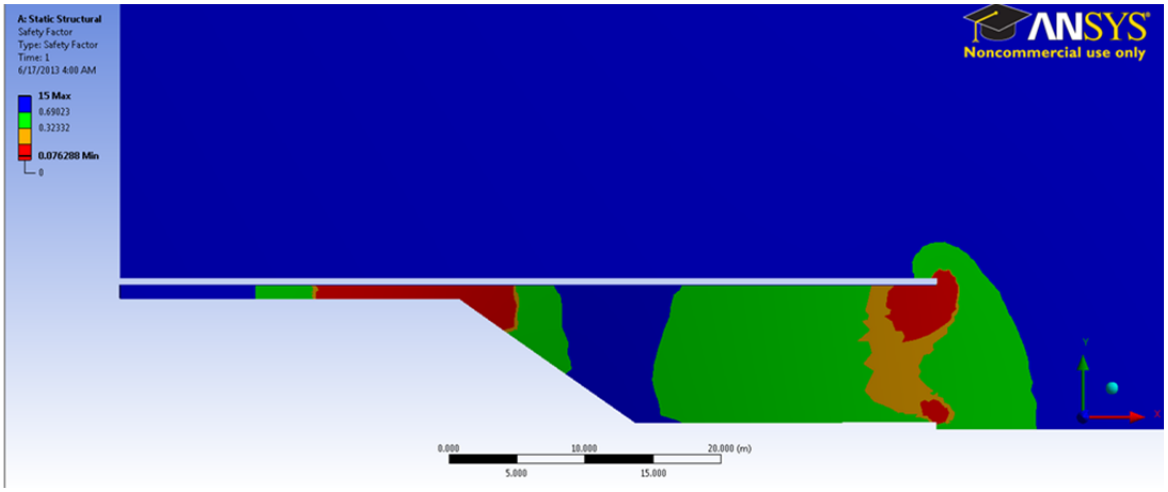

Figure 37. Bending failure stress contour for full penetration side and centerline cuts, located at the extreme breadth and stem of the icebreaker, respectively.

VI. CONCLUSIONS AND RECOMMENDATIONS

A. CONCLUSIONS

1. Hybrid Method

A hybrid method was developed such that ice resistance data from multiple sources may be cross-referenced or combined under common framework to better describe icebreaking in the analytical context. Within this framework, a numerical approximation for the bending ice resistance component was obtained via finite element model and related to existing analytical model with empirical basis in order to better understand the underlying physics as well as to improve the accuracy of existing ice resistance models. Upon achieving low error for given predefined influential parameters, the finite element ice sheets were damaged according to specified damage patterns, and this damage was accounted for as a decrease in the total ice resistance by using the Lindqvist analytical model.

2. Damaged Ice Sheet Resistance

The finite element model of the ice sheet was altered according to eight damage scenarios to relate any change in the bending stress failure contour to the bending resistance component. The method presented in this study indicates that the bending resistance is significantly reduced when the ice is damaged by either full penetration cuts, or cuts extending ahead of the icebreaker stem. The reduction of bending resistance for the centerline cut is particularly interesting because this is also the location of the breadth-independent stem crushing component. It may be possible to reduce the stem crushing component as well as the bending resistance for centerline cuts in the ice. Since the stem crushing and bending resistance components are likely coupled, this study was unable to account for any reduction in the stem crushing resistance while solving for the bending resistance. The present finite element static structural model could not account for stress gradient or stress rate failure criteria for the ice sheet because these values are not well represented in literature.

B. FUTURE WORK

To proceed with this work, both the time and size dependent failure properties of sea ice must be obtained. Without this information, it was impossible to numerically model the transient failure of ice and test against empirical data. In addition, further tests must be performed to quantify resistance component coupling in the hybrid model framework so that analytical methods may be further refined. If, for instance, the coupling between the stem crushing and bending resistance components are resolved, the effects of ice damage on the stem crushing component may be pursued.

APPENDIX A. LINDQVIST SENSITIVITY ANALYSIS

Each parameter in the Lindqvidst resistance formula was varied across a reasonable range of values, with respect to the vessels used by Lindqvist to formulate the method. The figures below illustrate the effect of this variation on the individual resistance components.

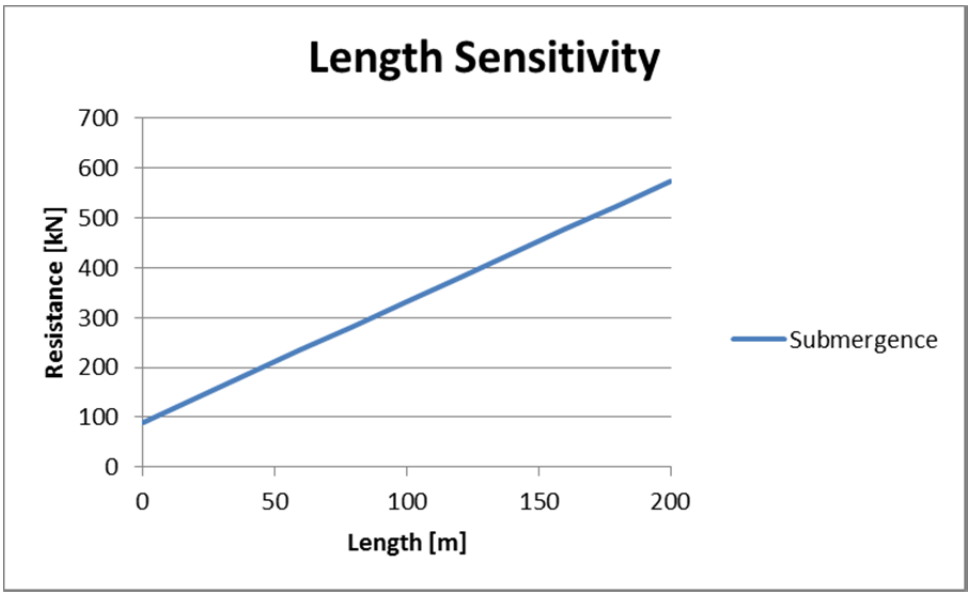

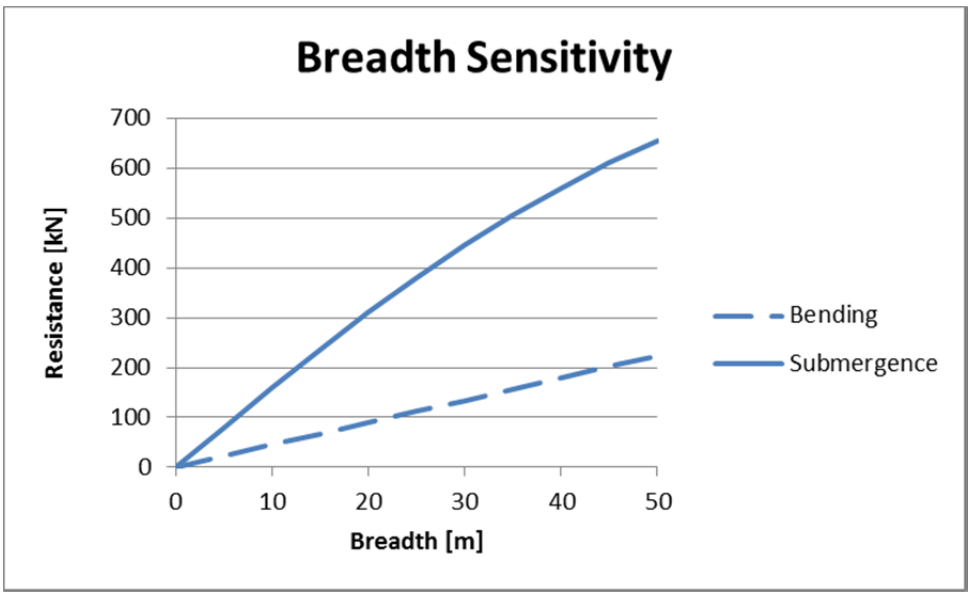

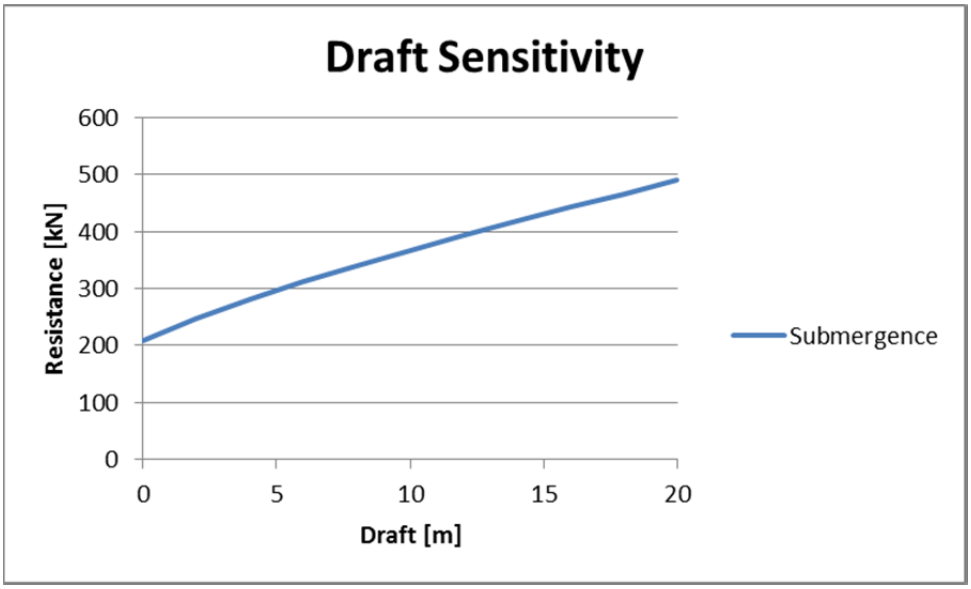
Draft Sensitivity
Resistance [kN]
600
500
400
300
200
100
0
0
5
10
15
20
Draft [m]
Submergence

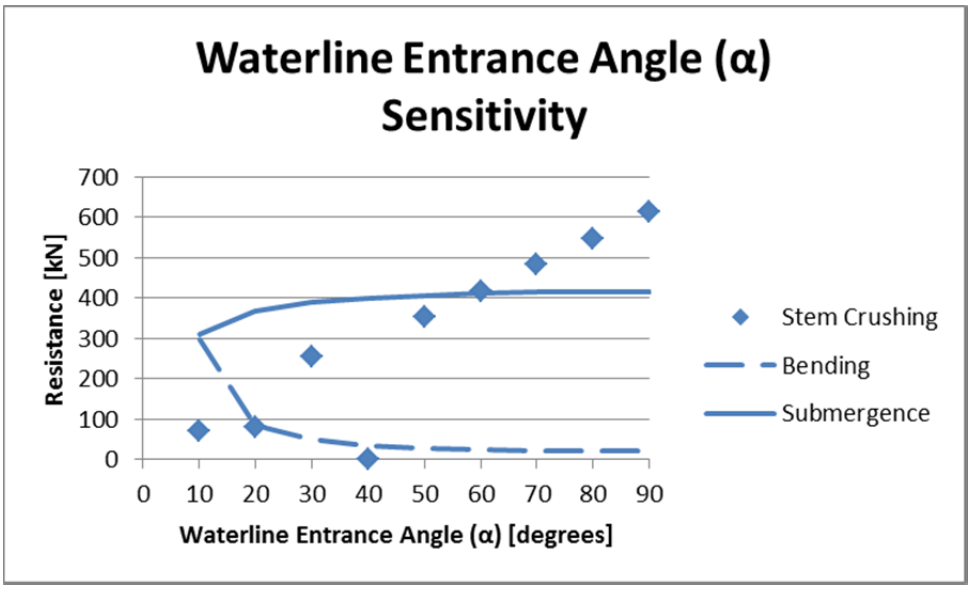
Waterline Entrance Angle (α) Sensitivity
Resistance [kN]
700
600
500
400
300
200
100
0
0
10
20
30
40
50
60
70
80
90
Waterline Entrance Angle (α) [degrees]
Stem Crushing
Bending
Submergence

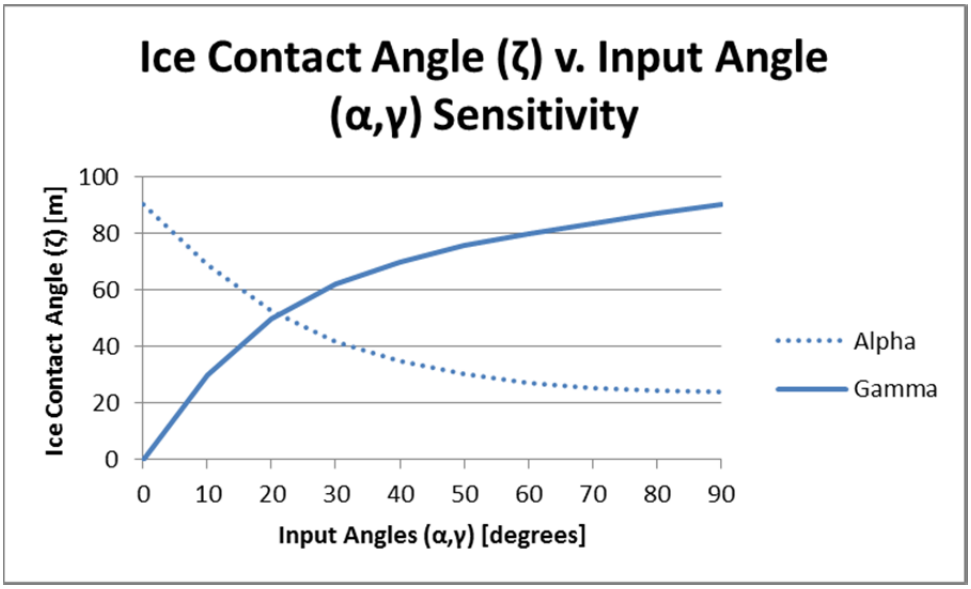
Ice Contact Angle (ζ) v. Input Angle (α,γ) Sensitivity
Ice Contact Angle (ζ) [m]
100
80
60
40
20
0
0
10
20
30
40
50
60
70
80
90
Input Angles (α,γ) [degrees]
Alpha
Gamma

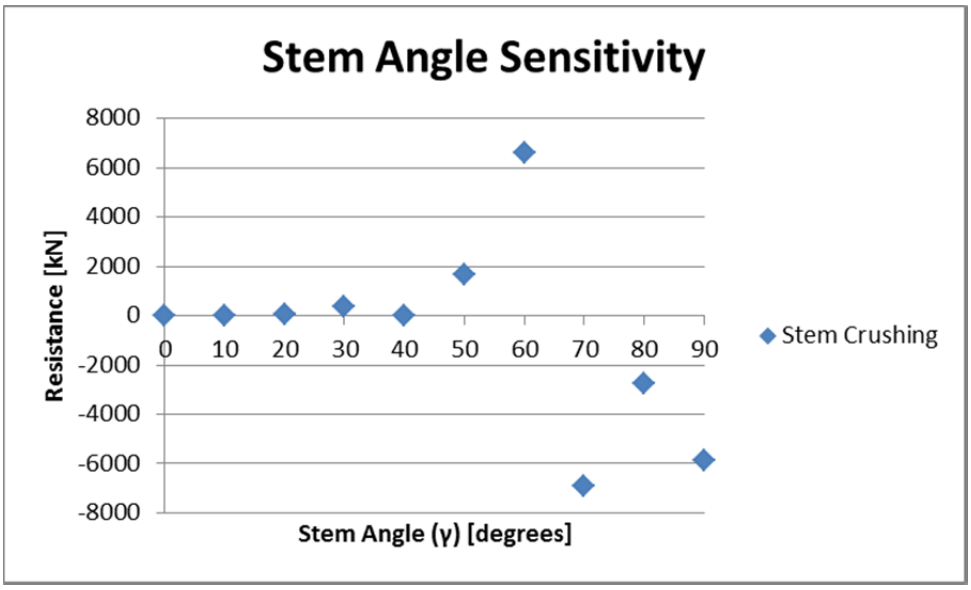
Stem Angle Sensitivity
Resistance [kN]
8000
6000
4000
2000
0
-2000
-4000
-6000
-8000
0
10
20
30
40
50
60
70
80
90
Stem Angle (γ) [degrees]
Stem Crushing

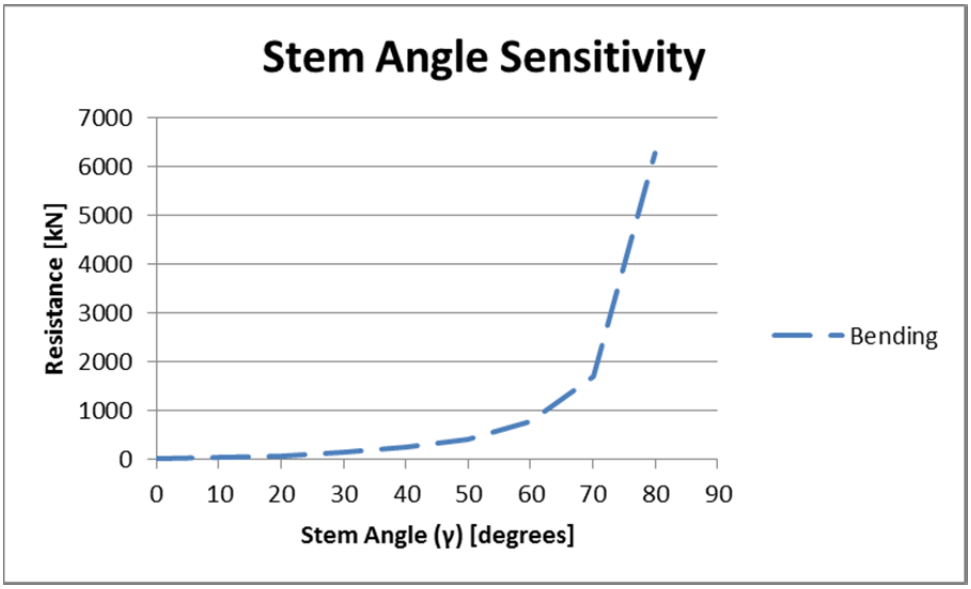
Stem Angle Sensitivity
Resistance [kN]
7000
6000
5000
4000
3000
2000
1000
0
0 10 20 30 40 50 60 70 80 90
Stem Angle (γ) [degrees]
Bending

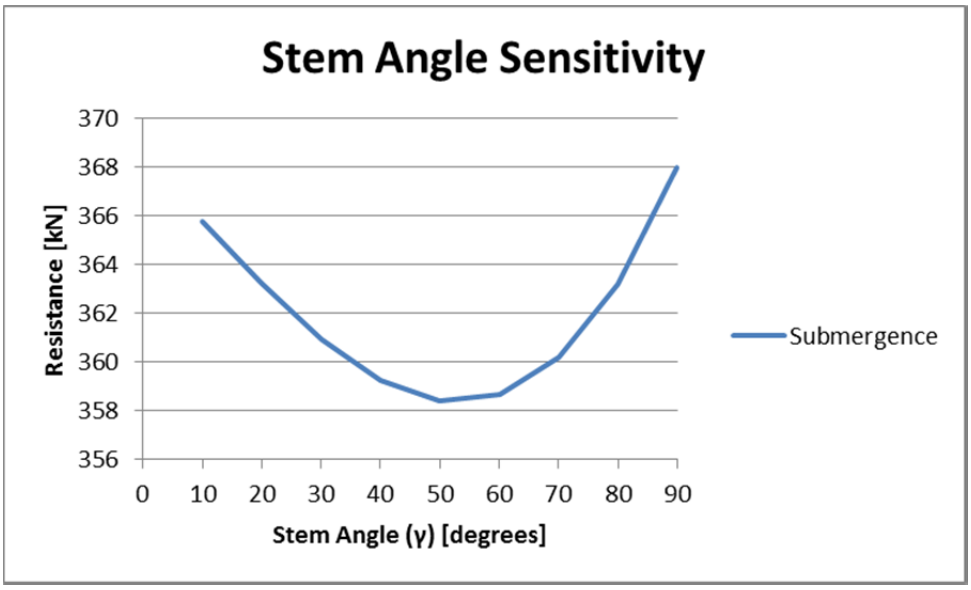
Stem Angle Sensitivity
Resistance [kN]
370
368
366
364
362
360
358
356
0 10 20 30 40 50 60 70 80 90
Stem Angle (γ) [degrees]
Submergence

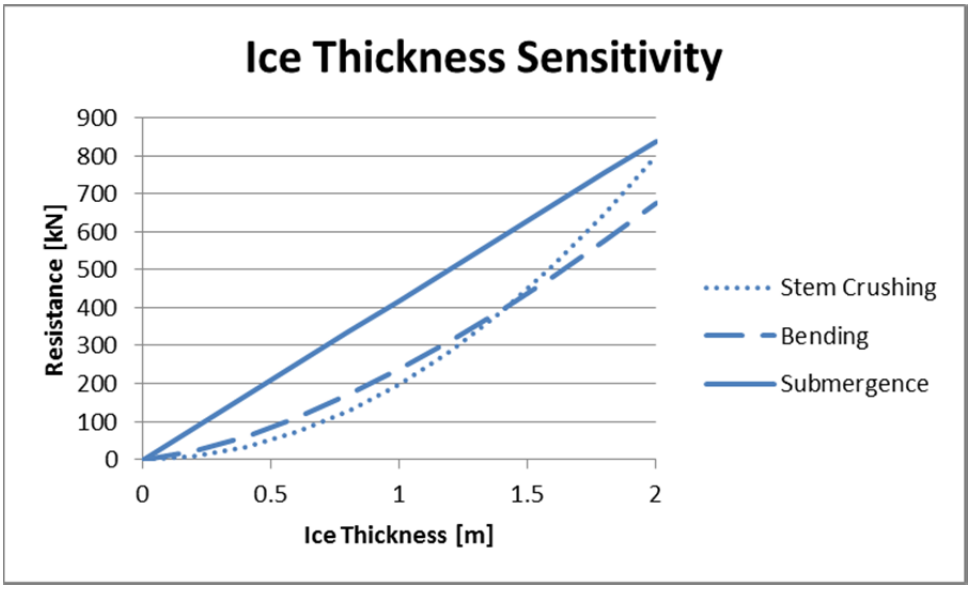
Ice Thickness Sensitivity
Resistance [kN]
900
800
700
600
500
400
300
200
100
0
0
0.5
1
1.5
2
Ice Thickness [m]
Stem Crushing
Bending
Submergence

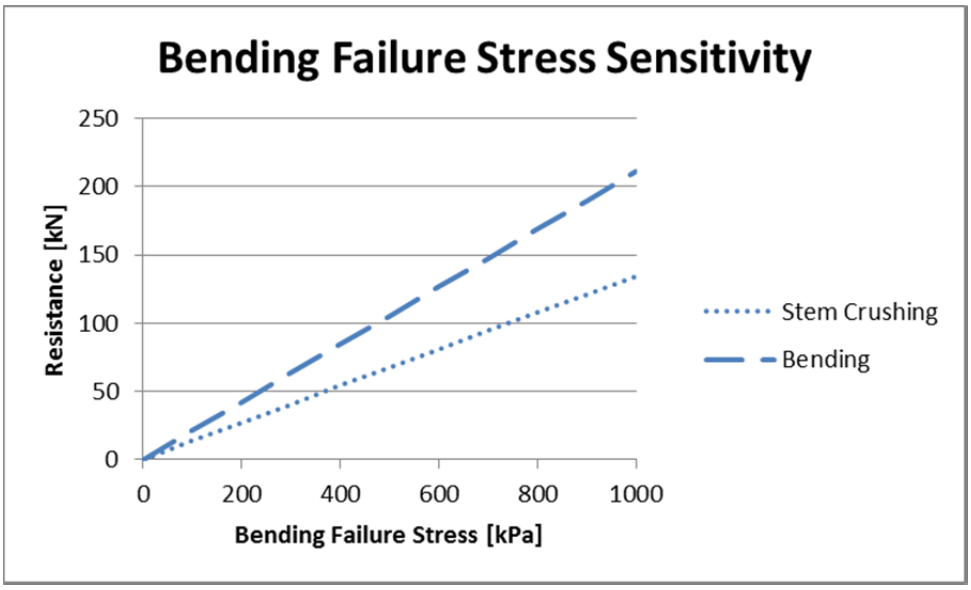
Bending Failure Stress Sensitivity
Resistance [kN]
250
200
150
100
50
0
0
200
400
600
800
1000
Bending Failure Stress [kPa]
Stem Crushing
Bending

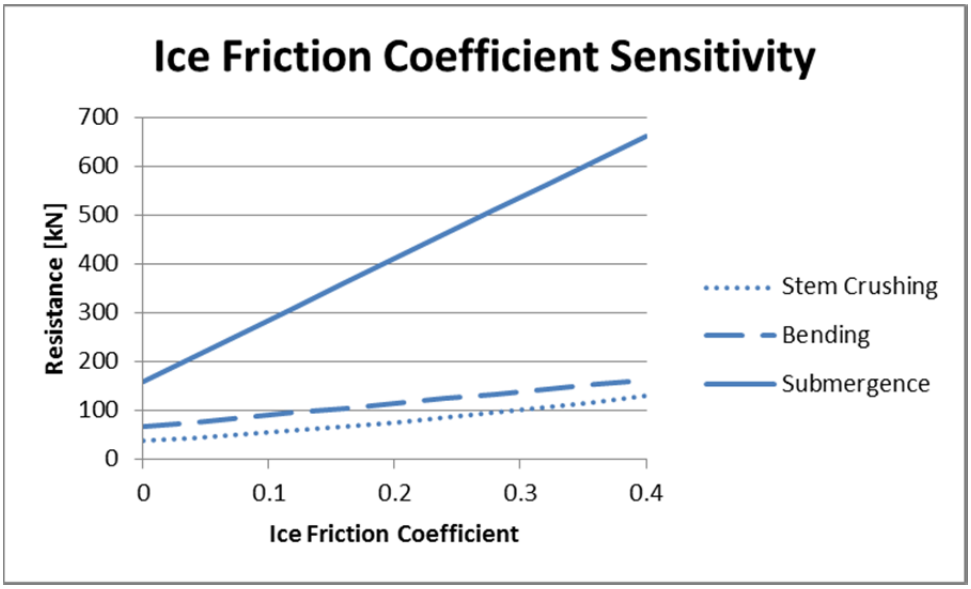
Ice Friction Coefficient Sensitivity
Resistance [kN]
700
600
500
400
300
200
100
0
0
0.1
0.2
0.3
0.4
Ice Friction Coefficient
Stem Crushing
Bending
Submergence

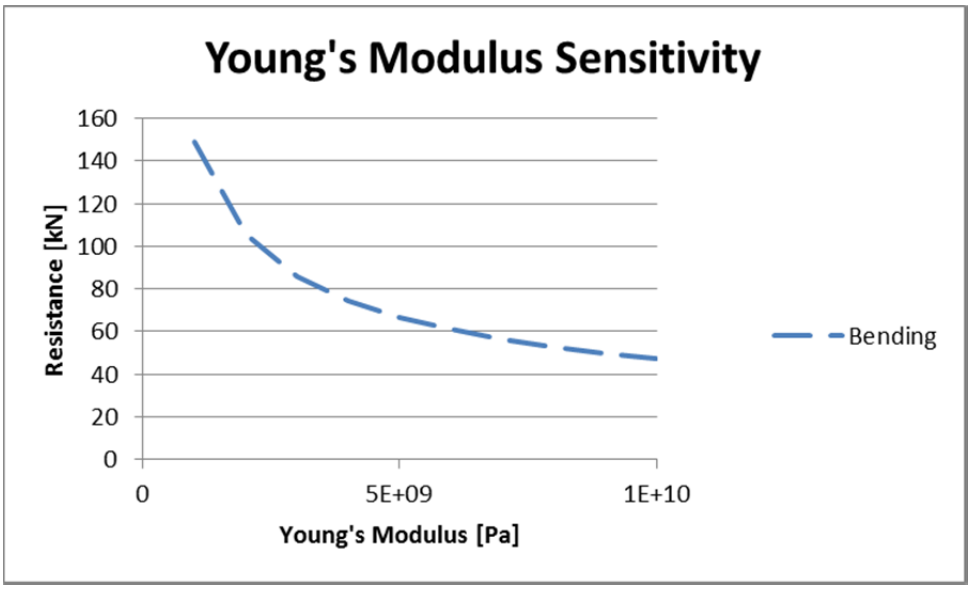
Young's Modulus Sensitivity
Resistance [kN]
160
140
120
100
80
60
40
20
0
0
5E+09
1E+10
Young's Modulus [Pa]
Bending

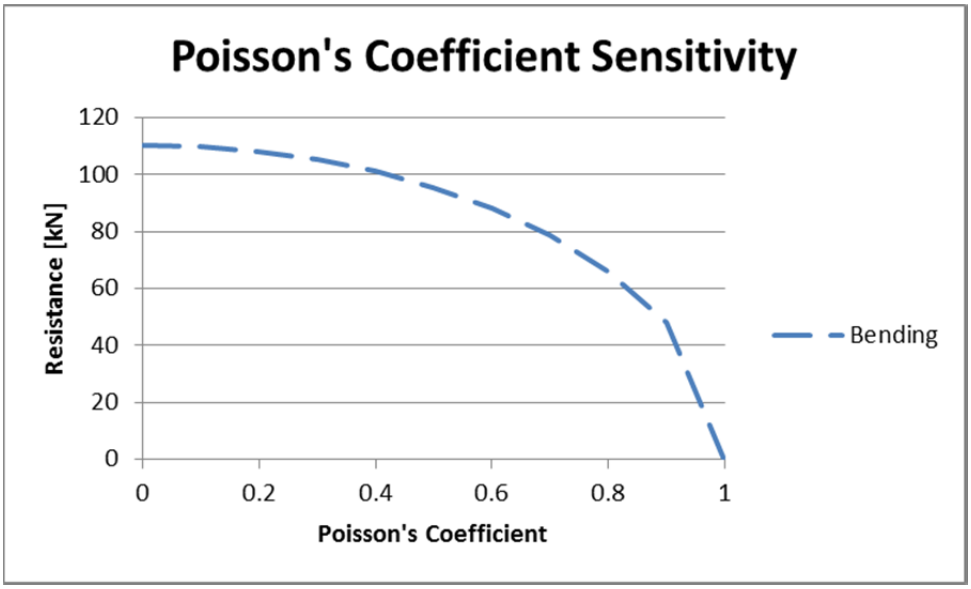
Poisson's Coefficient Sensitivity
120
100
80
60
40
20
0
Resistance [kN]
0
0.2
0.4
0.6
0.8
1
Poisson's Coefficient
Bending

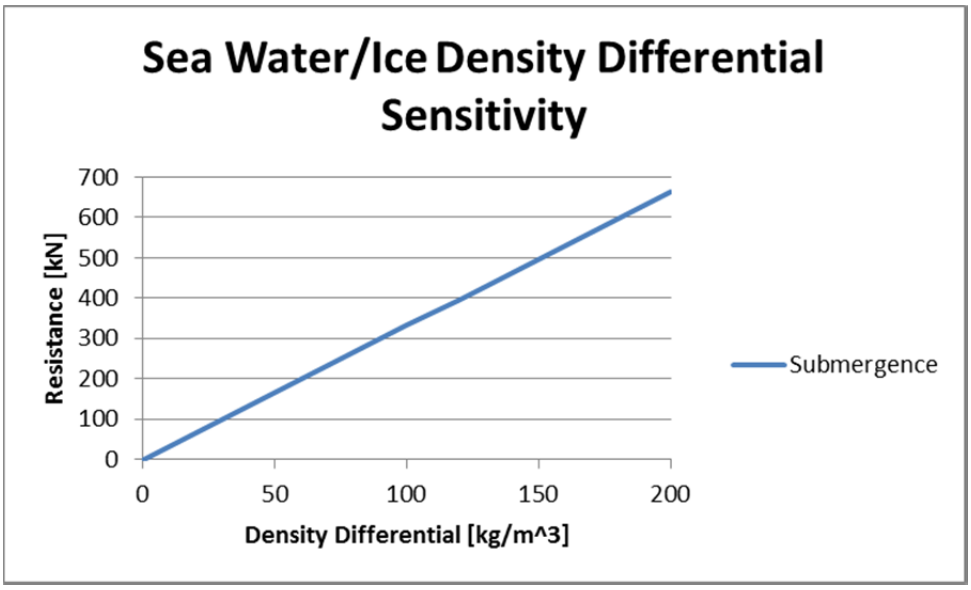
Sea Water/Ice Density Differential Sensitivity
700
600
500
400
300
200
100
0
Resistance [kN]
0
50
100
150
200
Density Differential [kg/m^3]
Submergence

THIS PAGE INTENTIONALLY LEFT BLANK

APPENDIX B. NUMERICAL ICEBREAKING VELOCITY MATLAB CODE

```
close all
clear all
clc

% Icebreaker Vladivostok
% Parameters
L = 112;
B = 23.5;
T = 9.5;
alpha = 18; % waterline entrance angle
gamma = 24; % stem angle
zeta = 56; % effective ice contact angle
mu = 0.16;

H = 0.58;
Hsnow = 0.28;
E = 2E9;
nu = 0.3;
sigmab = 500;
sigmac = 3430;
rhow = 1026;
deltarho = 109;

m = 5000;
g = 9.81;
Fpmin = 0;
Fpmax = 1400;

Fv = 84.1;
Rc = 67.25344;
Rb = 105.383;
Rs = 360.9507;

lc = (E*H^3/(12*(1-nu^2)*rhow*g))^0.25;
l = lc/3;
lx = l/sind(alpha);
lxn = 10;
lxi = lx/lxn;

a = Fv/(sigmac*10^3*B);
ax = a/sind(alpha);
axn = 10;
axi = ax/axn;

s = ax+lx;
sn = axn+lxn;

n = B/(l*sind(alpha));
```

```
Fbmax = Rb*(ax+lx)/(2*ax);

for k = Fpmin:Fpmax
    Fp = k;
    Fprop(k-Fpmin+1,1) = Fp;
    i = 1;
    Vn = 1.5;
    Vs = 0;
    Vsf = 1;
    while Vsf-Vs > 0.05
        for j = 1:axn
            Vs = Vn;
            Fb = Fbmax/axn*j;
            Rci = Rc*(1+1.4*Vn/sqrt(g*H));
            Rbi = Fb*(1+1.4*Vn/sqrt(g*H));
            Rsi = Rs*(1+9.4*Vn/sqrt(g*L));
            Vi(j,i) = Vn;
            Vo = Vi(j,i);
            Vx = 2*axi/m*(Fp-Rci-Rbi-Rsi)+Vo^2;
            Vi(j+1,i) = sqrt(Vx);
            Vn = Vi(j+1,i);
            V(j+(i-1)*(sn+1)) = Vn;
        end
        for j = axn+1:sn+1
            Vi(j,i) = Vn;
            Fb = 0;
            Rci = Rc*(1+1.4*Vn/sqrt(g*H));
            Rbi = Fb*(1+1.4*Vn/sqrt(g*H));
            Rsi = Rs*(1+9.4*Vn/sqrt(g*L));
            Vo = Vi(j,i);
            Vx = 2*lxi/m*(Fp-Rci-Rbi-Rsi)+Vo^2;
            Vi(j+1,i) = sqrt(Vx);
            Vn = Vi(j+1,i);
            V(j+(i-1)*(sn+1)) = Vn;
        end
        Vsf = Vn;
        i = i+1;
    end
    Vss(k-Fpmin+1,1) = k;
    Vss(k-Fpmin+1,2) = mean(Vi(:,i-1));
end

plot(V)
%Lindqvist = [0 534;4.251 1400];
%plot(Vss(:,2),Vss(:,1))
%hold on
%plot(Lindqvist(:,1),Lindqvist(:,2))
```

APPENDIX C. HYBRID METHOD DEVELOPMENT ERROR

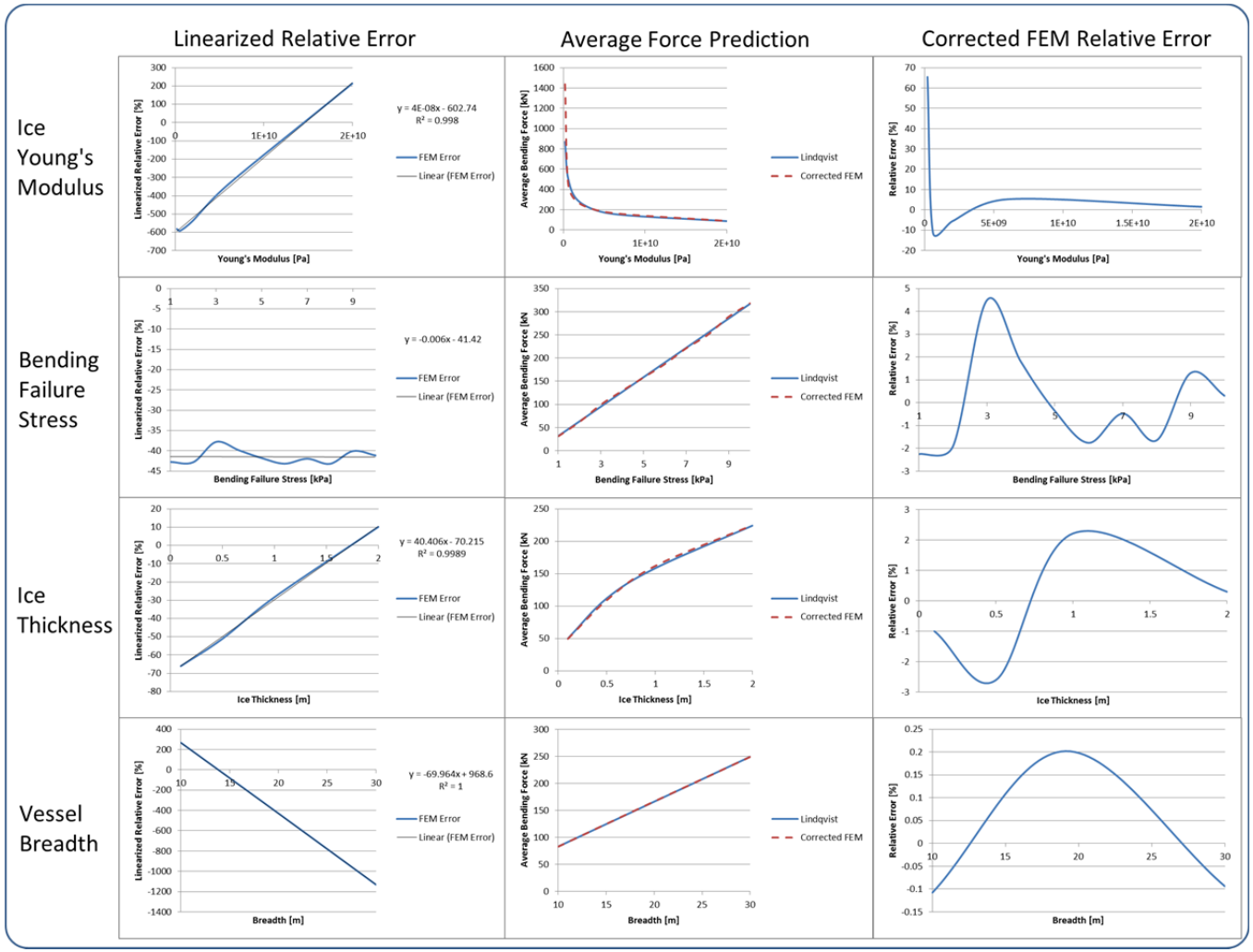

THIS PAGE INTENTIONALLY LEFT BLANK

LIST OF REFERENCES

[1] S. O. Makarov, "The yermak icebreaker," *The Geographical Journal*, vol. 15, no. 1, pp. 32–46, Jan. 1900.

[2] International Association of Classification Societies, "Requirements concerning polar class," *IACS Req. 2011.,* 2011, pp. (I1-1)-(I3-16).

[3] I. S. Peschanskiy, "Ice -cutting ships and high-pressure water jets for cutting ice," Defence Res. Board, Ottawa, Canada, Directorate of Physical Res., Rep. Misc. G-18 (84–315), 1964, pp. 1-5.

[4] R. Gragnon and M. Mellor, "Cutting ice with high pressure water jets," Natl. Tech. Info. Service, U.S. Dept. of Commerce, Springfield, VA, Rep. CG-D-15–73, 1973, pp. 1-32.

[5] Z. I. Shvaishtein, "Cutting ice with a continuous high-pressure water jet," Natl. Tech. Info. Service, U.S. Dept. of Commerce. Springfield, VA, 1973, pp. 1-15.

[6] M. Mellor, "Icebreaking concepts," U.S. Geological Survey, Dept. of Marine Geology, Hanover, NH, 1980, pp. 1-23.

[7] D. B. Coveney, "Cutting ice with high pressure water jets," Natl. Research Council Canada, Div. of Mech. Eng., Low Temp. Lab., Ottawa, Canada, Rep. NRC no. 19643, 1981, pp. 1-51.

[8] G. R. Gilbert *et al.*,"A multiattribute decision-making approach to the selection of an auxiliary device for icebreakers," USCG Res. and Develop. Center with New York State Department of Health and University of Colorado, Denver, 1982, pp. 240-252.

[9] A. Assur and W. Weeks, "The mechanical properties of sea ice," U.S. Army Mat. Comm., Cold Regions Res. and Eng. Lab., Hanover, NH, 1967, pp. 1-96.

[10] R. M. W. Frederking and M. Sayed, "An ice failure model incorporating size effects," Natl. Res. Council of Canada, Ottawa, Canada, 1989, pp. 596-605.

[11] Z. P. Bazant *et al.*, "Part-through bending cracks in sea ice plates: Mathematical modeling," *Ice Mech. 1995,* vol. 207, pp. 97–105, 1995, pp. 97-105.

[12] S. Kapustiansky *et al*., (1999). "*Numerical simulation of the ice failure process*," in *Proc. 15th Intl. Conf. Port Ocean Eng. Arctic Cond., 1999.*

[13] G. Lindqvist, "A straightforward method for calculation of ice resistance of ships," Wartsila Mar. Ind., Arctic Sea Trans., 1989, pp. 722-735.

[14] F. A. Geisel and R. P., Voelker, “Level ice resistance of uscg polar sea in Antarctica,” U.S. Dept. of Trans., Mar. Admin., Columbia, MD, Rep. 872C-2, 1984, pp. 1-97.

[15] R. Ettema *et al.*, “Dynamics of continuous-mode icebreaking by a polar-class icebreaker hull,” U.S. Dept. of Trans., Mar. Admin., Iowa Inst. of Hydr. Res., The Univ. of Iowa., Iowa City, IA, Rep. 314, 1987, pp. 1-186.

[16] P. Valanto, “A numerical model of the icebreaking process at the bow of a ship advancing in level ice,” Hamburg Ship Model Basin (HSVA), Hamburg, Germany, 1993, pp. 835-847.

[17] J. Martio, “Numerical simulation of vessel’s manoeuvering performance in uniform ice,” informally published manuscript, Ship Laboratory, Helsinki University of Technology, Espoo, Finland. 2007, pp. 1-30.

[18] T. Moan *et al*., “*Numerical simulation of ships operating in level ice*,” in *Proc. 21st Intl. Conf. Port Ocean Eng. Arctic Cond.* 2011, pp. 1-12.

[19] M. Lau *et al*., “Mathematical modeling of ice-hull interaction for ship maneuvering in ice simulations,” Mem. Univ. of Newfoundland and Inst. for Ocean Tech., St. John’s, Newfoundland, Canada, 2006, pp. 1-8.

[20] D. E. Nevel, “The narrow infinite wedge on an elastic foundation,” U.S. Army Corps of Eng., Snow Ice and Permafrost Res. Est., Wilmette, IL, Tech. Rep. 56, 1958, pp. 1-20.

[21] T. Skar, “Ice induced resistance of ship hulls: A comparison of resistance estimated from measurements and analytical formulations,” MS thesis, Norwegian Univ. of Sci. and Tech., Trondheim, Norway, 2011, pp. 1-126.

[22] I. B. Thorsen, “Estimation and computation of ice-resistance for ship hulls,” MS thesis, Norwegian Univ. of Sci. and Tech., Trondheim, Norway, 2012, pp. 1-158.

INITIAL DISTRIBUTION LIST

1. Defense Technical Information Center
   Ft. Belvoir, Virginia

2. Dudley Knox Library
   Naval Postgraduate School
   Monterey, California